Counter-current imbibition and non-linear diffusion in fractured porous media

F. Douarche, B. Braconnier, S. Momeni, M. Quintard, B. Nœtinger

Counter-current imbibition and non-linear diffusion in fractured porous media: Analysis of early- and late-time regimes and application to inter-porosity flux

F. Douarche[a], B. Braconnier[b], S. Momeni[a], M. Quintard[c] and B. Nœtinger[a,*]

[a]IFP Energies nouvelles, Earth Sciences and Environmental Technologies Division, 1 et 4 avenue de Bois Préau, Rueil-Malmaison, 92852, France
[b]IFP Energies nouvelles, Digital Sciences and Technologies Division, 1 et 4 avenue de Bois Préau, Rueil-Malmaison, 92852, France
[c]Institut de Mécanique des Fluides de Toulouse, UMR 5502 CNRS, Toulouse INP-ENSEEIHT, University of Toulouse III Paul Sabatier, Allée du Professeur Camille Soula, Toulouse, 31400, France

ARTICLE INFO

Keywords:
Multiphase flow
Capillary imbibition
Non-linear diffusion
Fractured porous media
Inter-porosity flux

ABSTRACT

The displacement of non-aqueous phase liquid (NAPL) in permeable porous rock by water saturating the surrounding fractures is studied. In many situations of practical interest, capillarity is the dominant driving force. Using the *global pressure* concept, it is shown that the water saturation is driven by a generic non-linear diffusion equation governing the matrix block counter-current spontaneous imbibition. In addition, in most cases, the saturation-dependent diffusion coefficient vanishes at the saturation end points, that renders the driving equation highly singular.

In this paper, two exact asymptotic solutions valid for short and long times are presented, under the assumption that the conductivity vanishes as a power-law of both phase saturations at the extreme values of the fluid saturation.

Focusing on the late-time domain, the asymptotic solution is derived using an Ansatz that is written under the form of a power-law time decay of the NAPL saturation. In the spatial domain, this solution is an eigenvector of the non-linear diffusion operator driving the saturation, for a problem with Dirichlet boundary conditions. If the diffusion coefficient varies as a power law of the NAPL saturation, the spatial variations of the solution are given analytically for a one-dimensional porous medium corresponding to parallel fracture planes. The analytical solution is in very good agreement with results of numerical simulations involving various realistic sets of input transport parameters.

Generalization to the case of two- or three-dimensional matrix blocks of arbitrary shape is proposed using a similar Ansatz, solution of a non-linear eigenvalue problem. A fast converging algorithm based on a fixed-point sequence starting from a suitable first guess was developed. Comparisons with full-time simulations for several typical block geometries show an excellent agreement.

These results permit to set-up an analytical formulation generalizing linear single-phase representation of matrix-to-fracture exchange term. It accounts for the non-linearity of the local flow equations using the power-law dependence of the conductivity for low NAPL saturation. The corresponding exponent can be predicted from the input conductivity parameters. Similar findings are also presented and validated numerically for two- or three-dimensional matrix blocks. That original approach paves the way to research leading to a more faithful description of matrix-to-fracture exchanges when considering a realistic fractured medium composed of a population of matrix blocks of various size and shapes.

1. Introduction

In many situations, fluid transport processes in complex porous systems may be described by the solution of a non-linear diffusion equation with a diffusion coefficient that depends on the local concentration or saturation of the solute or phase of interest. In the geosciences context, that can be the case when considering NAPL[1] displacement by water in aquifers or hydrocarbon recovery in rock matrix [9, 22, 29, 39, 41, 21, 26]. In the context of soil mechanics, one derives semi-analytical or numerical solutions of the Richards equation describing unsaturated flows with such non-linear forms [8, 34, 35, 5]. Other systems may receive similar descriptions ranging from filtration to astrophysics, including compressible gas flows in porous media, granular media flows [18, 17], among others.

The non-linearity of the driving diffusion equation implies that most of standard methods based on superposition properties such as Green's functions and Fourier decomposition fail down. In addition, the popular assumption that the diffusion coefficient vanishes at the limiting saturations, sharing a power-law dependence with the saturation adds a mathematical difficulty [2]. In particular, singular behaviours are to be expected close to the forcing boundaries where the diffusion coefficient may vanish.

*Corresponding author
frederic.douarche@ifpen.fr (F. Douarche); benjamin.braconnier@ifpen.fr (B. Braconnier); sina.momeni@ifpen.fr (S. Momeni); michel.quintard@imft.fr (M. Quintard); benoit.noetinger@ifpen.fr (B. Nœtinger)
www.ifpen.fr (F. Douarche); www.ifpen.fr (B. Braconnier); www.ifpen.fr (S. Momeni); www.imft.fr (M. Quintard); www.ifpen.fr (B. Nœtinger)
ORCID(s): 0000-0001-5943-6405 (F. Douarche); 0000-0003-1705-4892 (B. Braconnier); 0000-0002-8774-3709 (S. Momeni); 0000-0002-6150-7011 (M. Quintard); 0000-0002-4002-351X (B. Nœtinger)

[1]Hydrocarbons in liquid or gaseous state, pollutants, organic compounds, air…

In order to be more specific, in the geosciences context such a generic problem arises when considering a counter-current capillary imbibition process on a finite size matrix block approximated by a layer of length L embedded in a fracture network of high conductivity [22, 29, 41, 26]. The most standard approach to account for the presence of fractures is to adopt a dual-porosity description that involves two averaged equations for the macro-scale fracture and matrix effective media, in which some exchange term needs to be modeled [3, 16, 37, 25, 14]. In the single-phase case, the simplest model is the pseudo-steady-state dual-porosity model, that can be improved to account for additional internal matrix relaxation times using a time convolution with some kernel that is the solution of a linear diffusion problem on a representative matrix block [25, 30]. Such convolution models are not practical in numerical modeling but retain the multiple time-scales which are naturally observed.

Dual-porosity models involving a linear closure (local inter-porosity flux proportional to pressure/saturation/concentration difference) imply an exponential relaxation of the average quantity of interest, i.e. a single relaxation time. The associated characteristic time corresponds to the diffusion time over the matrix size $\tau_0 = L^2/D_0$, defined using some representative diffusion coefficient D_0 and a representative matrix block size L. At short times, a "boundary layer" behaviour is observed and can be estimated using the standard Boltzmann transformation, leading to a matrix-to-fracture flux varying as $1/\sqrt{t}$ [17, 26]. This regime may be observed while the diffusion distance remains lower than the typical size of the matrix blocks.

Fewer results are reported regarding the long time regime description occurring when water has invaded most of the pore volume of the rock. Using an overall dual-porosity description with a linear closure leads to first-order differential equations for the description of the matrix-fracture exchange, the solution of which implies an exponential relaxation of the NAPL saturation at long times [39]. That is reminiscent of the dual-porosity solutions obtained while interpreting pumping tests in fractured formations. The associated relaxation time still involves a characteristic diffusion time τ_0 conveniently weighted by a dimensionless shape factor that characterizes the overall matrix block geometrical shape [25].

In order to account more accurately for non-linear effects, an alternative approach is to change the analytical form of the exchange term by looking for a form involving a non-linear function of the average matrix block saturation. Semi-analytical developments in that direction were proposed by [41, 26]: solving a weak form of the full problem at hand, the authors introduce an approximation of the late-time solution using a suitably chosen spatial Ansatz. The model predicts a power-law time decay of the NAPL average saturation in the blocks. The corresponding exponent may be related directly to the exponent involved in the local diffusion coefficient dependence with saturation. Both papers show a good agreement between experimental data and simulation results. For completeness, [26] proposed an explicit representation of the exchanges using a non-linear term valid over the entire time scale.

In the present paper, we develop an alternative approach for the late-time asymptotics, looking for solutions having a power-law time decay at every location of the matrix block. Following this assumption, a complete determination of the solution can be obtained. This solution, which compares very well with numerical solutions, can be useful to propose a non-linear formula relating the matrix to fracture exchange flux to the remaining average NAPL saturation in the matrix. Generalizations of our approach to more complex fractured media are discussed.

The paper is organized as follows: first, the generic problem to be solved is presented in Section 2.2, and the notations and driving equations are introduced in Section 2.3. In particular, it is shown that the emergence of a non-linear diffusion equation driving the time-evolution of water saturation is not limited to specific fracture network geometries. A straightforward derivation is provided using the concept of *global pressure* that allows to show that the mean fluid velocity vanishes under various geometrical and physical conditions.

Restricting ourselves to one-dimensional counter-current displacements, results of semi-analytical short-time analysis using Boltzmann transformation are reviewed shortly in Section 3. Then the long-time asymptotic solution is presented in Section 4, the spatial dependence of which can be fully determined analytically, still in the case of a one-dimensional matrix geometry. In both sections, these solutions are compared with numerical simulations carried out at both short and long times.

In Section 5, the time variation of the overall flux at the matrix boundary is studied. That allows to set-up a formulation of the exchange term accounting for the non linearity.

Coming back to 2D or 3D cases, the approach is generalized for *arbitrary matrix block shapes* in Section 6. The corresponding Ansatz that describes the space dependency of the asymptotic behaviour is solution of a non-linear steady-state eigenvalue problem. That solution can be evaluated numerically using a fast converging original fixed-point algorithm presented in Section 6.3. That solution plays the role of the analytical solution developed in the one-dimensional case. Comparisons to full simulations showing an excellent agreement are presented in Section 6.4 for various matrix block geometries, including the one-dimensional previous solution.

Section 7 concludes and an appendix detailing the numerical scheme used to solve the counter-current equation closes the article.

2. Analytical and numerical models

In this section, we present the mathematical model and the numerical solution that will be used as a reference.

2.1. Driving forces involved in matrix-fracture transfers and considered flow regime

In a network of diffuse fractures where flow is taking place, the exchange interaction with the matrix blocks delineated by the fracture network, as sketched in Fig. 1, involves four forces: gravity, viscous forces, capillarity and molecular diffusion. In the following we will assume on the one hand that the molecular diffusion forces, which are by far the weakest, are negligible. On the other hand we consider such a high permeability contrast between the fractures and the matrix that the overall pressure gradient acting on one matrix block through the fracture is negligible. This leaves capillarity and gravity as dominant forces.

The capillary length l_{cap} is defined as the length beyond which gravity becomes important [15]. In porous media, it can be estimated by comparing the Laplace pressure $(2\gamma\cos\theta)/R$, where γ is the interfacial tension between water and NAPL, θ is the contact angle and R is the characteristic capillary tube radius of the equivalent porous medium represented as a bundle of capillary tubes, to the gravity-driven hydrostatic pressure $\Delta\rho g h$, where $\Delta\rho = \rho_w - \rho_o$ is the density difference between water and NAPL, h denotes the matrix block height and g the gravity acceleration. Equating these two pressures, setting $R = \sqrt{8k/\phi}$ where k and ϕ denote the matrix block average permeability and porosity, defines the capillary length

$$l_{\text{cap}} = \frac{2\gamma\cos\theta}{\Delta\rho g R} = \frac{\gamma\cos\theta\sqrt{\phi}}{\Delta\rho g\sqrt{2k}}. \tag{1}$$

This capillary length, which corresponds to a block height such that gravity and capillary forces are balanced, i.e. a unit Bond number

$$\text{Bo} = \frac{\Delta\rho g h R}{2\gamma\cos\theta} = \frac{\Delta\rho g h\sqrt{2k}}{\gamma\cos\theta\sqrt{\phi}} = \frac{h}{l_{\text{cap}}}, \tag{2}$$

defines two regimes depending on whether $l_{\text{cap}} \lesseqgtr h$ or $\text{Bo} \lesseqgtr 1$. Gravity is negligible for block height $h \ll l_{\text{cap}}$ ($\text{Bo} \ll 1$). When this condition is met, it is as sought the fluid is in a zero-gravity environment and capillary effects dominate. The opposite case, when $h \gg l_{\text{cap}}$ is referred to as the gravity regime ($\text{Bo} \gg 1$).

In what follows we consider only the capillary regime, that is rock-fluid configurations such that the block height is much lower than the capillary length, $h \ll l_{\text{cap}}$. **??** gives a few examples. For instance, assuming NAPL is a light oil, $\phi = 0.1$ and $\theta = \pi/3$, one gets a capillary length of about $l_{\text{cap}} \sim 4-9$ m for $k = 10$ mD, depending on temperature and pressure conditions. Basically, we are considering blocks of small height of the order of a few tens of centimeters to one meter.

2.2. Counter-current imbibition in the three-dimensional incompressible two-phase flow case without gravity

We start with general considerations about three-dimensional spontaneous counter-current capillary imbibition, then detail in Section 2.3 the corresponding one-dimensional problem under the same assumptions. We consider two-phase flow of incompressible fluids without gravity. Following the generalized multiphase Darcy's laws, the driving equations read [4]:

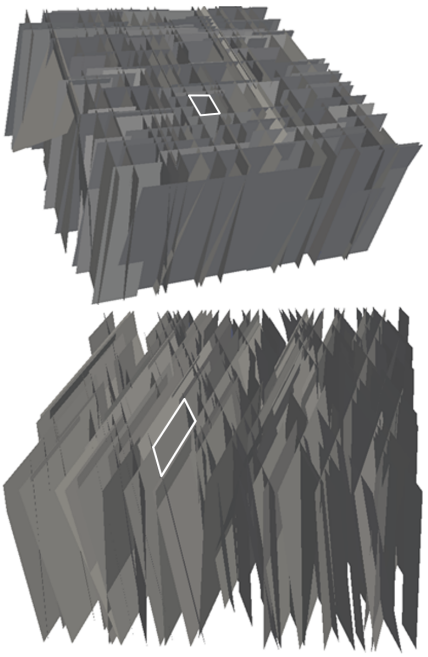

Figure 1: Examples of discrete fracture networks with two near-vertical fracture families (of mean spacing about 3 and 5 m). These fractured geometries delineate matrix blocks (not shown) of various shapes with two typical quadrangular contours shown in white that are the focus of this work (adapted from [21]).

$$\phi\frac{\partial S_w}{\partial t} - \nabla\cdot(k\lambda_w\nabla P_w) = 0, \tag{3}$$

$$\phi\frac{\partial S_o}{\partial t} - \nabla\cdot(k\lambda_o\nabla P_o) = 0, \tag{4}$$

$$S_w + S_o = 1, \tag{5}$$

$$P_o - P_w = P_c(S_w), \tag{6}$$

where ϕ and k denote the porosity and the permeability of the porous medium under consideration (here and in the following we assume that the permeability tensor is isotropic), $S_w(\mathbf{x},t) \in [S_{wi}, 1-S_{orw}]$ is the aqueous phase saturation, $S_o(\mathbf{x},t) \in [S_{orw}, 1-S_{wi}]$ is the non-aqueous phase saturation, S_{wi} is the connate (immobile) aqueous phase saturation, S_{orw} is the residual (immobile) non-aqueous phase saturation, $\lambda_\varphi(S_w) = k_{r\varphi}(S_w)/\mu_\varphi$ is the phase φ mobility where $\varphi = w, o$ denotes the aqueous and the non-aqueous phase respectively, $k_{r\varphi}$ is the relative permeability to phase φ, μ_φ is phase φ viscosity, P_φ the intrinsic average pressure in phase φ, and $P_c(S) = P_o - P_w$ is the capillary pressure between the non-aqueous and aqueous phases.

It is useful to introduce the concept of global pressure P_t that depends implicitly on position $\mathbf{x}$ and time t introduced

by [11, 12, 13, 20]:

$$P_t = P_w + \int_{S_i}^{S} \frac{\lambda_o}{\lambda_t} \frac{\mathrm{d}P_c}{\mathrm{d}S'} \mathrm{d}S', \tag{7}$$

where $\lambda_t = \lambda_w + \lambda_o$ is the total mobility and $S \in [0,1]$ the normalized mobile aqueous phase saturation defined as

$$S(\mathbf{x},t) = \frac{S_w(\mathbf{x},t) - S_{wi}}{1 - S_{orw} - S_{wi}} \tag{8}$$

where the mobile saturation range $1-S_{orw}-S_{wi}$ is non-zero. Global pressure is defined up to an arbitrary constant which is accounted for by choosing S_i that is an arbitrary saturation value in $[0,1]$. With some algebraic manipulations, the original set of equations (3)-(6) can thus be transformed as

$$\nabla \cdot \mathbf{u}_t = 0, \tag{9}$$

$$\mathbf{u}_t = -k\lambda_t \nabla P_t, \tag{10}$$

$$\phi \frac{\partial S_w}{\partial t} + \nabla \cdot \left(\frac{\lambda_w}{\lambda_t} \mathbf{u}_t + k \frac{\lambda_w \lambda_o}{\lambda_t} \nabla P_c \right) = 0, \tag{11}$$

where $\mathbf{u}_t = \mathbf{u}_w + \mathbf{u}_o$ denotes the total Darcy velocity, with $\mathbf{u}_\varphi = -k\lambda_\varphi \nabla P_\varphi$ and $\varphi = w, o$. Equation (10) can be derived from equations (3)-(6) and using equation (7) defining global pressure. It can be noticed that $\lambda_t \nabla P_t = \lambda_w \nabla P_w + \lambda_o \nabla P_o$. Global pressure may be interpreted as a pressure which would give, for a fictitious fluid with mobility λ_t equal to the sum of the mobilities of aqueous and non-aqueous phases, a flux equal to the sum of the flux of the aqueous and non-aqueous phases.

Combining Eqs (9) and (10), one is led to solve a quasi-Laplace equation that reads $\nabla \cdot (k\lambda_t \nabla P_t) = 0$ to be solved on the matrix domain with given boundary conditions. Imposing the rather general boundary conditions at the boundaries of the block, i.e. uniform pressure and saturation, we obtain that the global pressure (7) P_t is uniform at the block boundaries. Thus it can be shown that the unique solution of the quasi-Laplace equation fulfilling these boundary conditions is a constant: P_t does not depend on position. Therefore,[2] the total velocity vanishes: $\mathbf{u}_t = \mathbf{0}$. This result requires the absence of gravity effects, incompressible fluids, and the matrix permeability k may be heterogeneous. Setting $\mathbf{u}_t = \mathbf{0}$ in Eq. (11) shows that the saturation is driven by the following non-linear diffusion equation:

$$\frac{\partial S}{\partial t} = \nabla \cdot [D(S) \nabla S], \tag{12}$$

$$D(S) = -\frac{k}{\phi(1-S_{orw}-S_{wi})} \frac{\lambda_w(S)\lambda_o(S)}{\lambda_t(S)} \frac{\mathrm{d}P_c(S)}{\mathrm{d}S}. \tag{13}$$

That result shows that counter-current imbibition is not restricted to one-dimensional cases. Up to our knowledge, that result as well as its direct derivation introducing the global pressure for 2D or 3D situations under quite general conditions appear to be original and shows this non-linear diffusion equation is likely to describe the water saturation evolution in many situations of interest.

[2] This result can be derived using a variational formulation of Laplace equation.

2.3. Driving equations in the one-dimensional case

Spontaneous counter-current capillary imbibition of a one-dimensional matricial porous medium block of size L initially saturated with a non-aqueous phase that is drowned in water can be described, neglecting gravity and assuming the two phases are incompressible, as the non-linear diffusion equation (12) for the normalized mobile aqueous phase saturation (8) with initial condition $S = 0$ for all $x \in [0, L]$ and $t = 0$ and boundary conditions $S = 1$ for $x = 0$ and $x = L$ for all $t > 0$.

In order to analyze the early- and late-time behaviours, we express $D(S)$ as a function of the mobile aqueous phase saturation S (mobile non-aqueous phase saturation being $1 - S$) setting the relative permeabilities to the aqueous and non-aqueous phases and the capillary pressure as Brooks-Corey saturation power laws [7]:

$$k_{rw}(S) = \kappa_w S^p, \tag{14}$$

$$k_{ro}(S) = \kappa_o (1-S)^q, \tag{15}$$

$$P_c(S) = P_e / S^{1/m}, \tag{16}$$

where p, q and m are positive exponents, κ_φ is the maximum relative permeability to phase φ, and P_e is the entry pressure of the porous medium under consideration. While specifying relative permeabilities and capillary pressure saturation dependence is certainly a restriction, it should be noted that Brooks and Corey relationships are widely used for many rock types. In addition, it does not matter what the choice is as long as a power-law behavior is obtained at long times for $S \to 1$ (this last statement is less true regarding the early-time regime, which is not the major contribution of this paper, as it is discussed later). We highlight this by making a more versatile choice, later at the end of this section. The diffusion coefficient $D(S)$ given in Eq. (12) then writes

$$D(S) = D_0 \frac{S^r(1-S)^q}{MS^p + (1-S)^q} = D_1 \frac{S^r(1-S)^q}{S^p + \frac{1}{M}(1-S)^q}, \tag{17}$$

with

$$D_0 = \frac{k\kappa_w P_e}{m\phi\mu_w(1-S_{orw}-S_{wi})} = M D_1, \tag{18}$$

$$M = \frac{\mu_o \kappa_w}{\mu_w \kappa_o} = \frac{\lambda_w(S=1)}{\lambda_o(S=0)}, \tag{19}$$

$$r = p - \frac{m+1}{m}, \tag{20}$$

where M denotes the end-point mobility ratio between the aqueous and the non-aqueous phases, defined as the maximum aqueous phase mobility k_{rw}/μ_w, taken at $S = 1$, over the maximum non-aqueous phase mobility k_{ro}/μ_o, taken at $S = 0$ [6].

It is worth noting that Eq. (12) is of singular type for $r > 0$ or $q > 0$ because $D(S)$ cancels with either the aqueous phase mobility for $S = 0$ or the non-aqueous phase mobility for $S = 1$. It means that mathematical singularities can be expected near the boundary where $D \to 0$ for $S \to 0$, as well as in the long-time limit inside the rock for which $D \to 0$ for $S \to 1$. A singular regime can be expected at very short times too, due to the sharp jump of the water saturation from 1 to 0 near the boundary.

Clearly, the balance of forces at play that lies in a capillary pressure difference between the fracture (where $P_c = 0$) and the matrix (where $P_c \neq 0$) media commands that a flow is established and terminates when the equilibrium condition $P_c(S) = 0$ is reached, i.e. $S(x,t) = 1$ or $S_w(x,t) = 1 - S_{orw}$. Noteworthy, a non-zero solution of Eq. (12) should satisfy the boundary condition $(\partial S/\partial x)_{x=0} = -\infty$ and therefore present a vertical asymptote at the front face of the porous medium. Indeed, this is a necessary condition to get a non-zero fracture-to-matrix flux $(D(S)\,\partial S/\partial x)_{x=0}$ while D cancels at the boundary.

Thereafter, two limiting cases are particularly useful to consider: on the one hand, the case where $S \to 0$, which corresponds to the early-time counter-current spontaneous imbibition of the non-aqueous-phase-saturated block by an aqueous phase, and, on the other hand, the case where $S \to 1$, which corresponds to the late-time imbibition of the same type. For early- and late-time regimes, $D(S)$ behaves asymptotically as

$$D(S) \sim \begin{cases} D_0\, S^{\alpha_0} & \text{with } \alpha_0 = r \text{ for } S \to 0, \\ D_1\,(1-S)^{\alpha_1} & \text{with } \alpha_1 = q \text{ for } S \to 1. \end{cases} \quad (21)$$

Thus each of these two limiting cases reduces to a non-linear diffusion equation of the singular type with a power-law $D(S)$. Specifically, one gets for $S \to 0$

$$\frac{\partial S}{\partial t} = \frac{\partial}{\partial x}\left(D_0 S^{\alpha_0} \frac{\partial S}{\partial x} \right), \quad (22)$$

and for $S \to 1$

$$\frac{\partial (1-S)}{\partial t} = \frac{\partial}{\partial x}\left[D_1 (1-S)^{\alpha_1} \frac{\partial (1-S)}{\partial x} \right], \quad (23)$$

where D_0, D_1, α_0 and α_1 are given in Eqs (18), (19), (20) and (21). Typical $D(S)$ curves are reported in Fig. 2.

Coming back to the general case, considering a matrix block Ω of boundary $\partial\Omega$ with initial boundary value problem $S(\mathbf{x},t) = 0$ in Ω for $t = 0$ and $S(\mathbf{x},t) = 1$ on $\partial\Omega$ for all $t \geq 0$, Eqs (22) and (23) read respectively

$$\frac{\partial S}{\partial t} = \nabla \cdot \left(D_0 S^{\alpha_0} \nabla S \right), \quad (24)$$

$$\frac{\partial (1-S)}{\partial t} = \nabla \cdot \left[D_1 (1-S)^{\alpha_1} \nabla (1-S) \right]. \quad (25)$$

Given the initial boundary value problem under investigation, the late-time regime has an expected limit $S \to 1$ when $t \to \infty$, the early-time regime has a more subtle behavior since the initial condition corresponds to a jump at $x = 0$ because of the boundary condition $S = 1$ and the initial condition $S = 0$. As a consequence, any series solution will feature a full spectrum of saturation functions. We come back to this point in Section 3.

To finish with, it is worth noting that relationships (21)-(23) still hold when considering more versatile relative permeabilities such as [28, 27]

$$k_{rw}(S) = \kappa_w \frac{S^p}{S^p + \beta(1-S)^u}, \quad (26)$$

$$k_{ro}(S) = \kappa_o \frac{(1-S)^q}{(1-S)^q + \gamma S^v}. \quad (27)$$

In this case one gets

$$D(S) = D_0 \frac{S^{p-\frac{m+1}{m}}(1-S)^q}{MS^p\left[(1-S)^q + \gamma S^v\right] + (1-S)^q\left[S^p + \beta(1-S)^u\right]}, \quad (28)$$

hence $D(S) \sim D_0 S^{p-\frac{m+1}{m}}/\beta$ for $S \to 0$ and $D(S) \sim D_0\,(1-S)^q/(M\gamma)$ for $S \to 1$, which is precisely Eq. (21) up to the dimensionless constants β and γ. Although this type of correlation has no physical basis, unlike power-law relative permeabilities (14)-(15) which can be derived by analogy with a bundle of capillary tubes [36, 10, 45, 46, 43, 44, 40, 38], it can nevertheless be useful when considering natural porous media for which power laws are not good enough to match measurements.

Our starting point is thus relatively general and is valid as long as an asymptotic power-law behaviour is obtained at the extreme saturations, independently of any detail at intermediate saturation values and regardless of any empirical correlation used.

3. Early-time solution

The goal of present work is to set-up a description of the fluid transfer valid for the whole time range. The literature is very abundant on the short time scale regime that can be assimilated to flow in a semi-infinite medium. We recall some outstanding works of [18, 34] that are relatively little cited nowadays, whereas they give very accurate fudge-factor-free solutions.

In the early-time regime, following [8, 18, 34] and references therein, the idea is to consider that the overall size of the block may be ignored, leading to considering a semi-infinite medium. That suggests to seek a solution using the Boltzmann variable $\xi = x/\sqrt{4D_0 t}$, with boundary conditions $S(0) = 1$, $S(\infty) = 0$ and $D(S(\infty))\,(\mathrm{d}S/\mathrm{d}\xi)(\infty) = 0$. That yields thus the following equation

$$\frac{\mathrm{d}}{\mathrm{d}\xi}\left(\frac{D(S)}{D_0} \frac{\mathrm{d}S}{\mathrm{d}\xi} \right) + 2\xi \frac{\mathrm{d}S}{\mathrm{d}\xi} = 0. \quad (29)$$

A remarkable fact observed by many authors [18, 9, 34, 22, 41, 17, 26] is that the solution of this equation has a finite toe located at a distance ξ_0 from the boundary that depends on the input parameters of the equation.

In order to go farther, the saturation dependence of $D(S)$ suggests to express ξ as a function of S. A further transformation allows to treat the case of a $D(S)$ function given by Eq. (17). Following [8, 34], Eq. (29) can be recast under the equivalent form

$$D(S) = -2D_0 \frac{\mathrm{d}\xi}{\mathrm{d}S} \int_0^S \xi\, \mathrm{d}S. \quad (30)$$

This form assumes the existence of a finite front ξ_0 for which the saturation and the flux, proportional to $D(S)\,\mathrm{d}S/\mathrm{d}\xi$, cancel out.

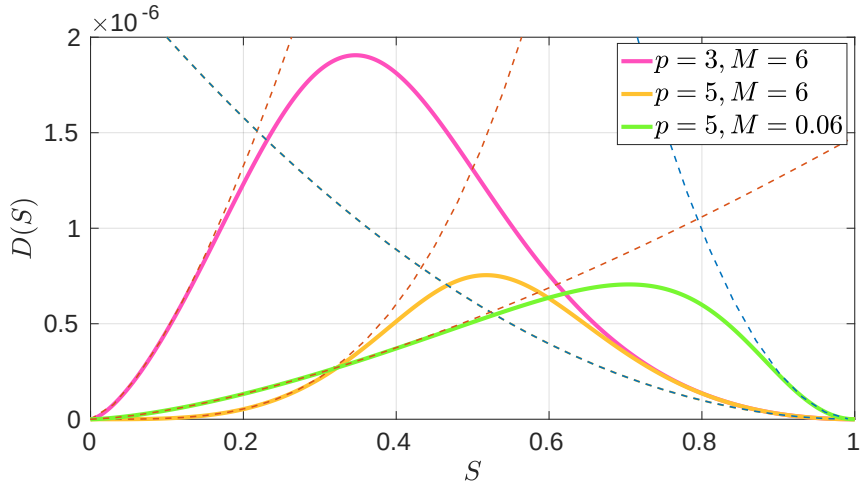

Figure 2: Several $D(S)$ given by Eq. (17) for $p = 3$, 5 and $M = 6$, 0.06 with $q = 2$, $m = 2$, $k = 10$ mD, $P_e = 5$ bar, $\phi = 0.25$, $S_{wi} = S_{orw} = 0$. Asymptotic power laws for the extreme saturations given by Eq. (21) are reported as dashed lines.

An iterative sequence of approximations [34] can be built by approximating the right-hand-side integral of Eq. (30) which yields, at the lowest order approximation

$$\frac{1}{2D_0}\int_0^S \frac{D(S')}{S'}\,\mathrm{d}S' \approx \xi_0(\xi_0-\xi), \tag{31}$$

and, at the higher order approximation

$$\frac{1}{2D_0}\int_0^S \frac{D(S')}{S'}\,\mathrm{d}S' \approx \xi_0(\xi_0-\xi) - \frac{A}{2}(\xi_0-\xi)^2, \tag{32}$$

where A is a constant equal to $1/(\alpha_0+1)$ for a power-law $D(S)$, which is approximately the case for a $D(S)$ function given by Eq. (17) if α_0 is large enough. The determination of ξ_0 follows directly from the boundary condition $S(\xi=0)=1$. These approximations provide an excellent accuracy not only in the neighborhood of ξ_0 for low saturation values.

In the power-law case, the solution proposed by [34] is consistent with the findings of [18] whose solution, later extended by [35], reads

$$S(\xi) = \begin{cases} [2\alpha_0\xi_0(\xi_0-\xi)]^{1/\alpha_0} f\left(\frac{\xi}{\xi_0}\right) & \text{if } \xi \in [0,\xi_0], \\ 0 & \text{if } \xi > \xi_0. \end{cases} \tag{33}$$

Here, the function $f(\xi/\xi_0)$ is a regular function that may be expressed as a power series of ξ/ξ_0 involving the exponent α_0 as a parameter [18].

The complete early-time saturation profile thus may be estimated analytically with an excellent accuracy, as reported in Fig. 3 which compares, for a few configurations, [34] solution (32) obtained by setting $A = 1/(\alpha_0+1)$ with the numerical solution obtained with the numerical scheme described in Appendix A. Saturation presents a vertical asymptote at the front face of the porous medium for $x = \xi = 0$ because a non-zero fracture-to-matrix flux $D(S)\,\partial S/\partial x = (D(S)/\sqrt{4D_0 t})\,\mathrm{d}S/\mathrm{d}\xi$ while $D(S) = 0$ for $S = 1$ at the boundary is only possible if $\partial S/\partial x = \mathrm{d}S/\mathrm{d}\xi = -\infty$. Flux vanishes as well at the toe position $\xi = \xi_0$ where $\mathrm{d}S/\mathrm{d}\xi = -2\xi_0[2\alpha_0\xi_0(\xi_0-\xi)]^{(1-\alpha_0)/\alpha_0} \sim 1/(\xi_0-\xi)^{(\alpha_0-1)/\alpha_0}$ [18], therefore the larger α_0 the sharper the front as shown in Fig. 3. To finish with, dimensional analysis suggests to normalize the timescale by the diffusion time $\tau_0 = L^2/(4D_0)$. Following our work objective, expressions for the matrix-to-fracture exchange term are investigated in Section 5.

4. Late-time asymptotic solution

Now, we focus on the late-time regime solution, for which the medium can no longer be assumed to be semi-infinite, and for which the authors have not found, to their best knowledge, any published exact solution.

An asymptotic solution for large t is sought using the Ansatz $1 - S(x,t) = y(x)/t^{\beta}$. Inserting this solution into Eq. (23) shows that this may be possible if the following condition is satisfied:

$$\beta = \frac{1}{\alpha_1}. \tag{34}$$

The asymptotic solution of Eq. (23) thus writes

$$1 - S(x,t) = \frac{y(x)}{t^{1/\alpha_1}}, \tag{35}$$

where $y(x)$ is a solution of the ordinary differential equation $\frac{\mathrm{d}}{\mathrm{d}x}\left(y^{\alpha_1}\frac{\mathrm{d}y}{\mathrm{d}x}\right) = -\frac{1}{\alpha_1 D_1}\,y$, which we shall rewrite

$$\frac{\mathrm{d}^2}{\mathrm{d}x^2}\,y^{\alpha_1+1} = -\frac{\alpha_1+1}{\alpha_1 D_1}\,y. \tag{36}$$

Further transformations $g = y^{\alpha_1+1}$ and $h = \lambda g$ with λ a constant yield

$$\frac{\mathrm{d}^2 h}{\mathrm{d}x^2} = -\lambda^{\frac{\alpha_1}{\alpha_1+1}}\,\frac{\alpha_1+1}{\alpha_1 D_1}\,h^{\frac{1}{\alpha_1+1}}. \tag{37}$$

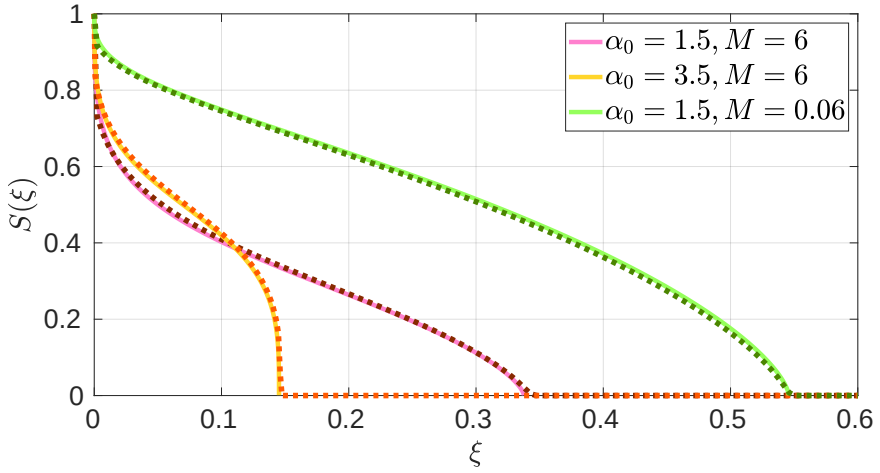

Figure 3: Comparison of early-time analytical solution given in Eq. (32) (solid lines) with the simulated one (dotted lines) for $\alpha_0 = 1.5,\ 3.5$ ($p = 3,\ 5$) and $M = 6,\ 0.06$ with $q = 2$, $m = 2$, $k = 10$ mD, $P_e = 5$ bar, $\phi = 0.25$, $S_{wi} = S_{orw} = 0$.

Choosing $\lambda = \left(\frac{\alpha_1 D_1}{\alpha_1+1}\right)^{\frac{\alpha_1+1}{\alpha_1}}$, Eq. (37) may be written under the following form:

$$\frac{\mathrm{d}^2 h}{\mathrm{d}x^2} = -h^{\frac{1}{\alpha_1+1}}, \tag{38}$$

$$h = \lambda g = \lambda y^{\alpha_1+1} = \left(\frac{\alpha_1 D_1}{\alpha_1+1}\right)^{\frac{\alpha_1+1}{\alpha_1}} y^{\alpha_1+1}. \tag{39}$$

For $x \in [0, L]$, boundary conditions $1 - S = 0$ for all $t > 0$ at $x = 0$ and $x = L$ yield $y(0) = y(L) = 0$, that is $h(0) = h(L) = 0$. The solution being symmetric around $x = L/2$, one must have $\mathrm{d}y/\mathrm{d}x > 0$ for $x \in [0, L/2]$ and $\mathrm{d}y/\mathrm{d}x < 0$ for $x \in [L/2, L]$. Therefore the condition $(\mathrm{d}y/\mathrm{d}x)(L/2) = 0$ must hold.

Before going further it is worth noting that Eq. (38) simplifies into $\mathrm{d}^2h/\mathrm{d}x^2 = -1$ when exponent α_1 is very large, whose solution is the parabola $h(x) = \frac{1}{2}x(L-x)$ such that $h(L/2) = L^2/8$.

Coming back to the general case, it can be remarked that multiplying each member of Eq. (38) by $\frac{\mathrm{d}h}{\mathrm{d}x}$, the equation can be integrated once to yield

$$\frac{1}{2}\left(\frac{\mathrm{d}h}{\mathrm{d}x}\right)^2 = \frac{\alpha_1+1}{\alpha_1+2}\left(h^{\frac{\alpha_1+2}{\alpha_1+1}}\left(\frac{L}{2}\right) - h^{\frac{\alpha_1+2}{\alpha_1+1}}\right), \tag{40}$$

where the right hand side $\frac{\alpha_1+1}{\alpha_1+2} h^{\frac{\alpha_1+2}{\alpha_1+1}}(\frac{L}{2})$ is an integration constant that is determined by the condition $\frac{\mathrm{d}h}{\mathrm{d}x}(\frac{L}{2}) = 0$. For $x \in [0, L/2]$, this last form integrates into

$$\begin{aligned} x &= \sqrt{\frac{\alpha_1+2}{2(\alpha_1+1)}} \int_0^h \frac{\mathrm{d}h}{\sqrt{h^{\frac{\alpha_1+2}{\alpha_1+1}}(\frac{L}{2}) - h^{\frac{\alpha_1+2}{\alpha_1+1}}}} \\ &= \sqrt{\frac{(\alpha_1+1)h^{\frac{\alpha_1}{\alpha_1+1}}(\frac{L}{2})}{2(\alpha_1+2)}} \int_0^{[h/h(\frac{L}{2})]^{\frac{\alpha_1+2}{\alpha_1+1}}} \frac{t^{\frac{\alpha_1+1}{\alpha_1+2}-1}}{\sqrt{1-t}}\,\mathrm{d}t, \end{aligned} \tag{41}$$

setting $t = \left[h/h(\frac{L}{2})\right]^{\frac{\alpha_1+2}{\alpha_1+1}}$. This relationship set with $x = \frac{L}{2}$ yields $h(\frac{L}{2})$ in implicit form:

$$\frac{L}{2} = \sqrt{\frac{(\alpha_1+1)h^{\frac{\alpha_1}{\alpha_1+2}}(\frac{L}{2})}{2(\alpha_1+2)}} \int_0^1 \frac{t^{\frac{\alpha_1+1}{\alpha_1+2}-1}}{\sqrt{1-t}}\,\mathrm{d}t. \tag{42}$$

Using Euler incomplete beta and gamma[3] functions, the solution rewrites as

$$x = \sqrt{\frac{(\alpha_1+1)h^{\frac{\alpha_1}{\alpha_1+1}}(\frac{L}{2})}{2(\alpha_1+2)}}\, B\left(\left[\frac{h}{h(\frac{L}{2})}\right]^{\frac{\alpha_1+2}{\alpha_1+1}}; \frac{\alpha_1+1}{\alpha_1+2}, \frac{1}{2}\right), \tag{43}$$

with $h(\frac{L}{2})$ given by

$$h\left(\frac{L}{2}\right) = \left(\frac{L}{2\sqrt{2\pi}} \frac{\alpha_1}{\sqrt{(\alpha_1+1)(\alpha_1+2)}} \frac{\Gamma(\frac{\alpha_1}{2(\alpha_1+2)})}{\Gamma(\frac{\alpha_1+1}{\alpha_1+2})}\right)^{\frac{2(\alpha_1+1)}{\alpha_1}}. \tag{44}$$

Noteworthy, this solution converges for $\alpha_1 \to \infty$ to the parabola that was previously obtained by direct calculation in the specific case of a very large α_1 exponent, which writes implicitly $x = L/2 - \sqrt{(L/2)^2 - 2h}$ with $h(L/2) = L^2/8$.

Going back to the main unknown y, related to h by Eq. (38), the following implicit expression that fulfills all the boundary conditions may be obtained:

$$x = \sqrt{\frac{\alpha_1 D_1\, y^{\alpha_1}(\frac{L}{2})}{2(\alpha_1+2)}}\, B\left(\left[\frac{y}{y(\frac{L}{2})}\right]^{\alpha_1+2}; \frac{\alpha_1+1}{\alpha_1+2}, \frac{1}{2}\right), \tag{45}$$

with $y(\frac{L}{2})$ given by

$$y\left(\frac{L}{2}\right) = \left(\frac{L}{2}\sqrt{\frac{\alpha_1}{2\pi(\alpha_1+2)D_1}} \frac{\Gamma(\frac{\alpha_1}{2(\alpha_1+2)})}{\Gamma(\frac{\alpha_1+1}{\alpha_1+2})}\right)^{\frac{2}{\alpha_1}}. \tag{46}$$

[3] Incomplete beta, beta and gamma function are respectively defined as [1] $B(x; a, b) = \int_0^x t^{a-1}(1-t)^{b-1}\,\mathrm{d}t$, $B(x, y) = \int_0^1 t^{x-1}(1-t)^{y-1}\,\mathrm{d}t = \frac{\Gamma(x)\Gamma(y)}{\Gamma(x+y)}$ and $\Gamma(z) = \int_0^\infty t^{z-1}e^{-t}\,\mathrm{d}t$.

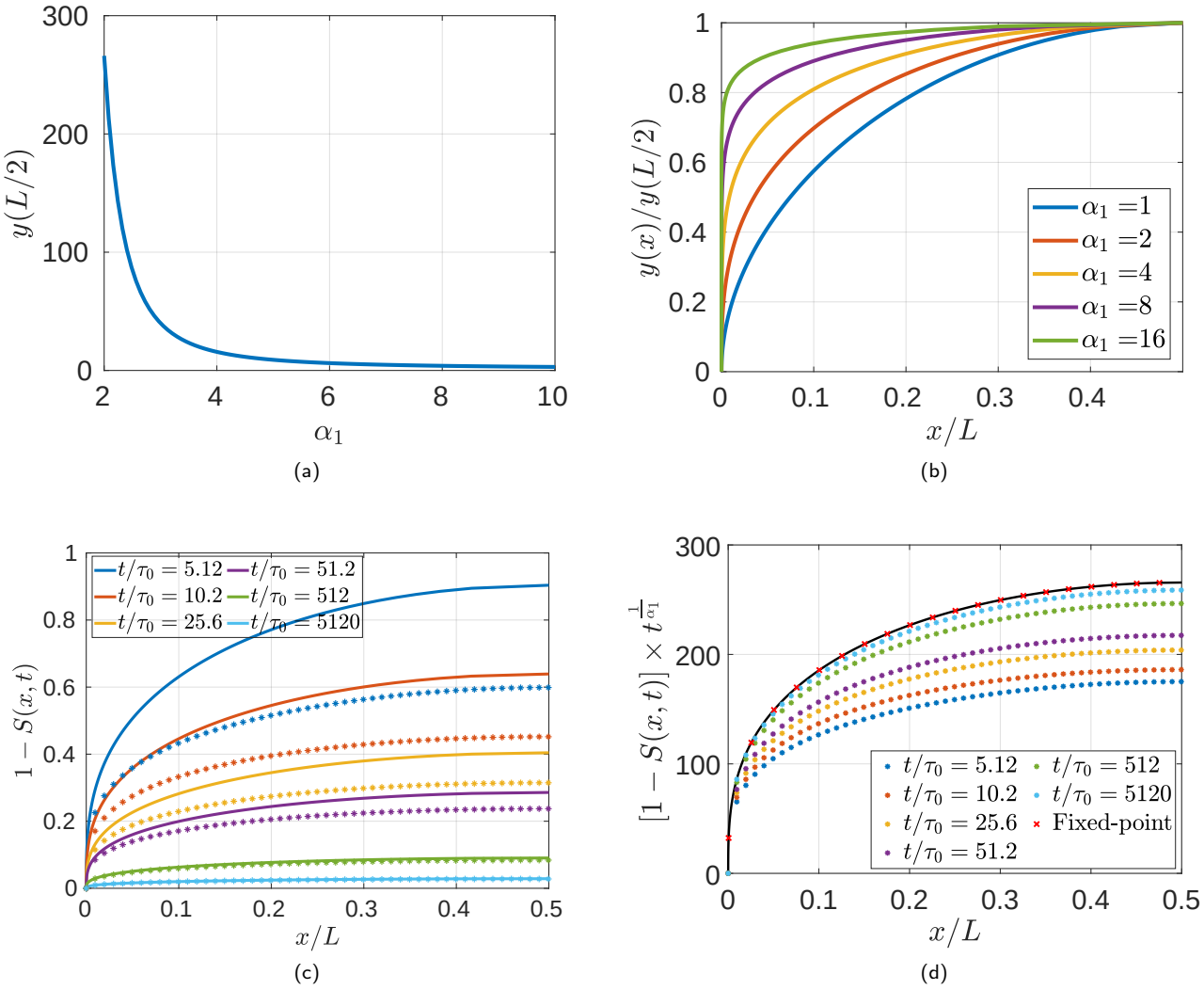

Figure 4: (a)-(b) Late-time analytical solution $y(x)$ given in Eqs (45)-(46) for several α_1 values. (c)-(d) Comparison of the late-time analytical solution $1 - S(x,t) = y(x)/t^{1/\alpha_1}$ and rescaled $y(x) = [1 - S(x,t)]\, t^{1/\alpha_1}$ (solid lines) given in Eqs (35), (45) and (46) with the simulated one (symbols) for $\alpha_1 = 2$, $p = 3$, $M = 6$, $m = 2$, $k = 10$ mD, $P_e = 5$ bar, $\phi = 0.25$, $S_{wi} = S_{orw} = 0$. Timescale is normalized by the diffusion time $\tau_0 = L^2/(4D_0)$. Red crosses for the fixed-point solution indicated in (d) correspond to a direct numerical solution of the asymptotic Ansatz detailed in Section 6.

The solution for $y(\frac{L}{2})$ and $y(x)/y(\frac{L}{2})$ are reported in Figs 4(a) and (b). Unlike solutions (32) and (33) obtained for the early-time regime by assuming the porous block to be semi-infinite, the late-time asymptotic solution (45) derived on a finite-size domain involves a characteristic length which is the block length L. Contrary to the early-time solution, in the late-time regime the water saturation is close to unity at every location in the matrix, therefore the power-law assumption given in Eq. (23) is automatically satisfied. A good agreement can be expected for the long time asymptotic behaviour independently of the details of $D(S)$ over the whole range of saturations, as reported in Figs 4(c)-(d) where the timescale is normalized by the diffusion time $\tau_0 = L^2/(4D_0)$.

In the displayed example, the time convergence of the numerical solution to the asymptotic one given in Eqs (35), (45) and (46) is pretty slow. That can be accurately quantified by comparing the time evolution of the numerical solution $1 - S$ or $(1 - S)\, t^{1/\alpha_1}$ with the asymptotic one for fixed x/L values. Specifically, the numerical solution time convergence to the asymptotic one is slower than the asymptotic solution $1/\sqrt{t}$ trend for $\alpha_1 = 2$ and intermediate t/τ_0 values. The reader may wish to consult Fig. 5 given later in Section 5, which reports the time evolution of the matrix-to-fracture flux, to spot the transition between the early- and the late-time regimes that occurs around $t/\tau_0 = 40$-50 in the example displayed in Figs 4(c)-(d). Ultimately, the numerical solution time evolution matches the asymptotic solution one as Figs 4(c)-(d) indicate about 7 and 2% relative difference between numerical and asymptotic solutions, $|S_\infty - S_{\text{num}}|/(1 - S_\infty)$, for $t/\tau_0 = 512$ and 5120, respectively. The larger the exponent α_1, the slower this

convergence. This is consistent with the typical behaviour of a porous medium that is preferentially wettable to the non-aqueous phase, for which the exponent $q = \alpha_1$ of the relative permeability to the non-aqueous phase, assuming a power-law saturation dependency (14)-(16), is generally large, for it imbibes more slowly than a water-wet porous medium.

To conclude this section, unlike the early-time regime, in the late-time regime, the low NAPL assumption $S(t) \approx 1$ becomes more and more valid as time increases. The asymptotic solution is likely to be independent on the details of $D(S)$ once $D(S) \approx D_1 (1-S)^{\alpha_1}$ as $S \to 1$.

5. Towards a non-linear closure for matrix-to-fracture flux

When large discrete fracture networks embedded in a permeable porous matrix are considered, it is customary to adopt a dual-porosity framework in which the coupling with the matrix may be accounted for via a source term $\Phi_{\rm mf}(t)$ [25, 14, 32, 30, 33]. This source term $\Phi_{\rm mf}(t)$ corresponds to a volume average of the normal flux between matrix and fractures. In the case of linear local flow equations, the generic closure of $\Phi_{\rm mf}(t)$ appears as being a time convolution of the local variable $S(x,t)$ with a time-dependent kernel that may be evaluated solving a relaxation problem on a representative matrix block [25, 30, 33]. In particular, focusing on the long-time limit, when the relaxation of the block reaches its exponential decay, it can be shown that $\Phi_{\rm mf}(t) \approx -\frac{S(x,t)-S_{\rm f}(x,t)}{\tau_{\rm m}}$ with x the block centroid and $S_{\rm f}$ the surrounding fracture saturation. The relaxation time $\tau_{\rm m}$ may be related to the block typical dimensions via the relation $\tau_{\rm m} \approx \sigma L^2/D_0$ where σ is the so-called shape-factor of the matrix block. In the stratified case, $\sigma = 12$. In the more general case, it is a geometric quantity that is known for several block shapes, and that is related to the smallest eigenvalue of the Laplacian operator with Dirichlet boundary conditions on the block [25].

Coming back to the non-linear case, at first sight, the convolution approach is useless, so other closure must be proposed, if any. In both short- and long-time regimes, the time variation of the matrix to fracture flux $\Phi_{\rm mf}(t) = (D(S)\,\partial S/\partial x)_{x=0}$ can be estimated using the previously presented solutions. In the short-time case, using the Boltzmann variable, $\Phi_{\rm mf}(t)$ may be estimated directly as $\Phi_{\rm mf}(t) = (D(S)/\sqrt{4D_0 t})(\mathrm{d}S/\mathrm{d}\xi)_{\xi=0} \sim 1/\sqrt{t}$ up to a prefactor A_0. In the long-time case, it is useful to introduce the spatial average of the matrix saturation defined by $\langle S\rangle(t) = \frac{1}{L/2}\int_0^{L/2} S(x,t)\,\mathrm{d}x$. Averaging the diffusion equation (12) and swapping the time partial derivative and the spatial average, one gets $\frac{L}{2}\frac{\mathrm{d}\langle S\rangle}{\mathrm{d}t} = \int_0^{L/2}\frac{\partial}{\partial x}\left(D(S)\frac{\partial S}{\partial x}\right)\mathrm{d}x = -\left(D(S)\frac{\partial S}{\partial x}\right)_{x=0}$ hence $\Phi_{\rm mf}(t) = \frac{L}{2}\frac{\mathrm{d}\langle S\rangle}{\mathrm{d}t}$. In all the considered cases, similar results were obtained using the time derivative of the average saturation or the global flux at the boundary, so the former definition was retained. Inserting the late-time Ansatz in this expression, it may be shown that the matrix to fracture flux varies asymptotically as $\Phi_{\rm mf}(t) \sim 1/t^{(\alpha_1+1)/\alpha_1}$.

The proportionality factor A_∞ can be evaluated using the analytical solution $y(x)$ starting from equations (40) and (44). The same algebraic decay was already discovered by [41, 26]. In both papers, the authors selected Ansatz dealing with the spatial variable valid close to the matrix/fracture boundary. Although that approach leads to analogous long time variations of the NAPL saturation, it does not provide a complete solution in the space domain, and it appears less general, especially in the multi-dimensional case.

Summarizing the results, we get:

$$\Phi_{\rm mf}(t) \approx \begin{cases} A_0/\sqrt{t} & \text{for } t \to 0, \\ A_\infty/t^{\frac{\alpha_1+1}{\alpha_1}} & \text{for } t \to \infty. \end{cases} \tag{47}$$

Both constants A_0 and A_∞ encapsulate the spatial details of the corresponding asymptotic solutions and may be obtained manipulating the expressions (29) for A_0 and (39), (40), (43) and (44) to obtain A_∞, that gives the following expressions:

$$A_0 = \sqrt{D_0}\int_0^1 \xi(S)\,\mathrm{d}S, \tag{48}$$

$$A_\infty = \frac{1}{\alpha_1}\left(\frac{\alpha_1+1}{\alpha_1 D_1}\right)^{\frac{1}{\alpha_1}}\sqrt{\frac{2(\alpha_1+1)}{\alpha_1+2}}\times \times\left(\frac{L}{2\sqrt{2\pi}}\frac{\alpha_1}{\sqrt{(\alpha_1+1)(\alpha_1+2)}}\frac{\Gamma(\frac{\alpha_1}{2(\alpha_1+2)})}{\Gamma(\frac{\alpha_1+1}{\alpha_1+2})}\right)^{\frac{\alpha_1+2}{\alpha_1}}. \tag{49}$$

If one plots $\Phi_{\rm mf}(t)$ using a log-log scale, two straight lines can be observed. The transition time from one regime to the other corresponds to a time t such that $\xi_0 = L/2$.

This is illustrated in Fig. 5(a) which reports the time evolution of the matrix-to-fracture flux for a few $\alpha_{0,1}$ values. Simulated early- and late-time slopes are in excellent agreement with the early- and late-time predictions $\frac{1}{2}$ and $\frac{\alpha_1+1}{\alpha_1}$, respectively. The transition between the early- and late-time regimes, which is observed for $t/\tau_0 =$ 5-10 in Fig. 5(a) and is very clear with a very tight and sharp cross-over, could be rescaled to $t/\tau_0 = 1$ by considering not the characteristic time $\tau_0 = L^2/(4D_0)$ suggested by dimensional analysis but $\tau_0 = L^2/(16\xi_0^2 D_0)$ derived from $\xi = x/\sqrt{4D_0 t}$ setting $\xi = \xi_0$ and $x = L/2$. It is worth noting the low influence of the early-time exponent α_0.

Fig. 5(b) reports the time evolution of the simulated fracture-to-matrix flux $\Phi_{\rm mf}$ multiplied by its asymptotic time dependencies (47) and divided by its asymptotic prefactors A_0 and A_∞ (48) and (49) for the same α_0 and α_1 exponents as in Fig. 5(a). Except for the cross-over between the short and long time regimes, the asymptotic solutions (47) are found with excellent accuracy and dominate most of the exchange dynamics over several orders of magnitude.

It can be observed that using the long-time asymptotics $\langle S\rangle \sim t^{1/\alpha_1}$, one can write the matrix to fracture flux under the following form: $\Phi_{\rm mf}(t) \sim -\langle S\rangle^{\alpha_1+1}$. That non-linear closure between the local matrix to fracture flux and the average matrix saturation generalizes the usual linear closure

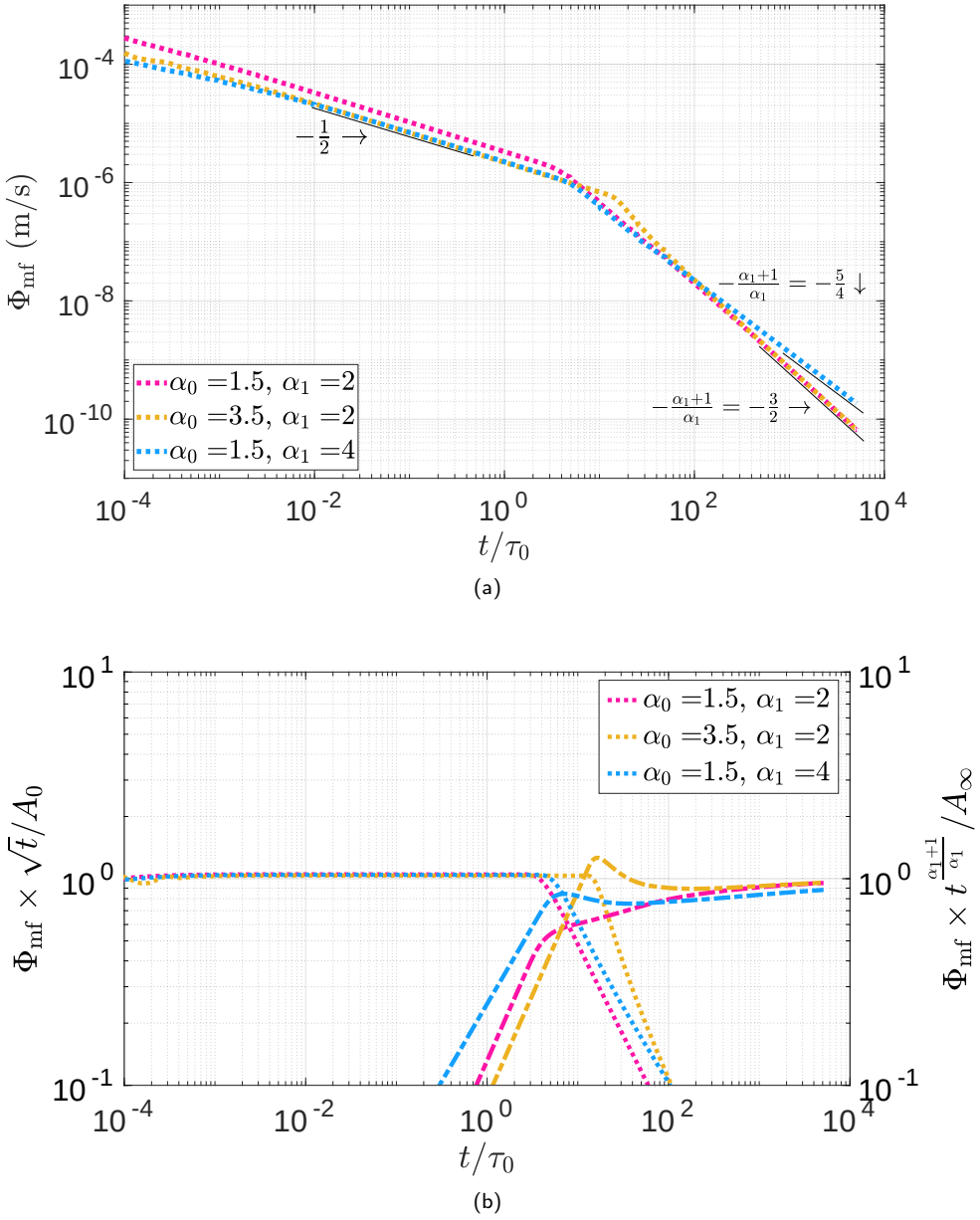

Figure 5: (a) Time evolution of the matrix-to-fracture flux for a few α_0 and α_1 exponents $\alpha_0 = 1.5, 3.5$ ($p = 3, 5$, $m = 2$) and $\alpha_1 = 2, 4$ with $M = 6$, $k = 10$ mD, $P_e = 5$ bar, $\phi = 0.25$ and $S_{wi} = S_{orw} = 0$. Simulated early- and late-time slopes $-\{0.48, 0.46, 0.44\}$ and $-\{1.45, 1.48, 1.21\}$, respectively, are in excellent agreement with the early- and late-time predictions (thin solid lines) $-\frac{1}{2}$ and $-\frac{\alpha_1+1}{\alpha_1} = -\frac{3}{2}$ and $-\frac{5}{4}$ for $\alpha_1 = 2$ and 4, respectively. Timescale is normalized by the diffusion time $\tau_0 = L^2/(4D_0)$. (b) Time evolution of the matrix-to-fracture flux multiplied by its asymptotic time dependencies (47) and divided by its asymptotic prefactors A_0 and A_∞ (48) and (49) for the same α_0 and α_1 exponents.

relation that gives rise to most dual-porosity models. The underlying proportionality factor may be obtained directly from the fixed-point solution that will be presented in Section 6, and could be related to usual shape factors of the literature [25].

To finish with, it can be remarked that using the relation $\Phi_{\rm mf}(t) = \frac{L}{2}\frac{{\rm d}\langle S\rangle}{{\rm d}t}$, if $\alpha_1 = 0$ is inserted in that formula, it provides an exponential relaxation of the matrix saturation. That is consistent with the corresponding findings of the constant diffusion case. In the non-linear case, a non-linear closure is obtained. Estimations of that closure for a whole range of time-scales accounting for both the short time and long time scales were proposed by [26].

6. Generalization to 2D or 3D matrix blocks

We now generalize the results obtained in one dimension of space to any dimension of space for any matrix

block geometry. Under the given boundary conditions, the porous medium still undergoes counter-current imbibition as demonstrated in Section 2.2 without the need for the matrix block to exhibit symmetries.

We first indicate in Sections 6.1 and 6.2 which quantitative features are preserved with respect to the one-dimensional early- and late-time asymptotic solutions and corresponding fluxes, and which are not and require additional investigation.

We show in Section 6.3 how the late-time asymptotic solution separate form (35) can be exploited to develop a simple and efficient fixed-point numerical solution method, which advantageously replaces the delicate solving of the initial nonlinear singular diffusion equation.

Finally, we demonstrate in Section 6.4, by considering some simple two-dimensional block geometries, that the full dynamics of capillary imbibition can be accurately and efficiently predicted. The matrix block imbibition still presents two regimes whose saturation and fracture-to-matrix flux can be computed: a diffusive early-time regime and an anomalous late-time regime that cross-over tightly. Eventually, residual points to investigate are discussed.

6.1. Early-time regime

In the general case of matrix blocks having arbitrary shapes, there is no simple approximation working yielding a detailed description of the short time regime. A generalization of Parlange's results might be worth investigating, although nothing simple is apparent at first sight. At very short time, keeping the Boltzmann assumption of a dependency on $\mathbf{x}/\sqrt{t}$ is equivalent to set-up a boundary layer approximation [23, 24, 42]. Physically it corresponds to consider that locally the block boundary can be assumed to be planar, and then to use the one-dimensional solution. Such an approximation can be assumed to be valid if the diffusion length $\sqrt{D_0 t}$ is much smaller than any characteristic lengthscale of the block. The occurrence of such a regime is confirmed once considering the matrix-to-fracture flux that is observed hereafter in Fig. 11 of Section 6.4 to vary as $1/\sqrt{t}$ at short times for simple matrix block geometries. Then a transient regime leading to the long time asymptotic solution can be observed.

6.2. Late-time regime

As detailed in the next section, the late-time asymptotic solution in the separate form (35) remains valid for any dimension of space and any block shape, except that the function $y(x)$, whose analytical expression (45) has been derived in one dimension of space, and which we will henceforth denote $f(\mathbf{x})$, remains to be determined. Thus, except for this detail which we will show hereafter how to manage quickly and accurately numerically, the late-time asymptotic solution $1 - S(\mathbf{x}, t)$ preserves a time dependence in $1/t^{1/\alpha_1}$ and the corresponding asymptotic flux (47) still presents an algebraic anomalous decay that is proportional to $1/t^{(\alpha_1+1)/\alpha_1}$, whose prefactor A_∞ remains to be computed and no longer writes as in (49) as it obviously depends on the space solution $f(\mathbf{x})$.

6.3. Fixed-point algorithm

The late-time asymptotic approach (35) remains valid for any dimension of space and any block shape. The solution of (25) writes

$$1 - S(\mathbf{x}, t) = \frac{f(\mathbf{x})}{t^{1/\alpha_1}} \tag{50}$$

where $f(\mathbf{x})$ satisfies $\nabla \cdot (f^{\alpha_1} \nabla f) = -f/(\alpha_1 D_1)$, which is rewritten as already done in Eqs (36)-(39)

$$\nabla^2 h = -h^{\frac{1}{\alpha_1+1}}, \tag{51}$$

$$h = \left(\frac{\alpha_1 D_1}{\alpha_1+1}\right)^{\frac{\alpha_1+1}{\alpha_1}} f^{\alpha_1+1}. \tag{52}$$

As already noted in Section 4, h satisfies $\nabla^2 h = -1$ when the exponent α_1 is very large, whose solution is a parabola in one dimension. This will serve as an initial guess to implement a fixed-point method to solve (51).

We are thus led to solve a Laplace equation in a domain Ω of boundary $\partial\Omega$ on which $h = 0$. Specifically, a sequence of functions $(h_k)_{k\geq 0}$ such that

$$\begin{aligned} \nabla^2 h_k &= -h_{k-1}^{\frac{1}{\alpha_1+1}} \quad \text{in } \Omega, \\ h_k &= 0 \qquad\qquad\quad \text{on } \partial\Omega, \end{aligned} \tag{53}$$

for all $k \geq 1$ is looked for with the following initial guess

$$\begin{aligned} \nabla^2 h_0 &= -1 \quad \text{in } \Omega, \\ h_0 &= 0 \qquad \text{on } \partial\Omega. \end{aligned} \tag{54}$$

At each iteration of the algorithm, we solve the non-singular elliptic problem (53) using a Newton-Raphson method embedded in the finite element method framework provided by the FreeFEM++ open-source PDE solver [19]. In 2D, that code generates meshes with triangular elements and Lagrangian P1 basis functions. The iterative algorithm is performed until $\|h_k - h_{k-1}\|_\infty$ and $\|h_k - h_{k-1}\|_2$ are small enough. Residuals less than 10^{-12} have been imposed so that a few iterations (about 20) are enough to converge which makes the algorithm fast and allows the use of fine meshes to obtain very accurate solutions. Also, as the initial guess corresponds to the solution of Eq. (54) with $\alpha_1 \to \infty$, a faster convergence is expected for higher values of α_1 for a given geometry.

6.4. Results

Running the algorithm in the one-dimensional case gives an excellent agreement with the analytical solution as reported in Fig. 4(d). A similar result has been obtained (but is not shown here as it does not bring much) by considering not the one-dimensional segment $[0, L]$ but a two-dimensional rectangle as shown in Fig. 6 with the same initial and boundary conditions, i.e. one pair of faces facing each other with imposed saturation and the other with zero flux.

Four two-dimensional geometries were considered in order to validate the fixed-point algorithm, considering the

saturation imposed on the whole boundary of the matrix block, from the most to the least symmetrical, as shown in Fig. 6:

- Disk of radius R,
- Square of side L,
- Rectangle of sides L_x and L_y,
- Quadrangle of medians L_x and L_y.

For the record, the spherical geometry has also been treated but is not reported because except for some elementary algebra details it does not differ significantly from the cylindrical geometry shown hereafter (both are systems with one degree of freedom).

In each case, the diffusion time is defined by $\tau_0 = L_c^2/(4D_0)$ where L_c is a characteristic length of the considered geometry, that is $L_c = 2R$, L or L_x or L_y depending on whether the medium is a disk, square, rectangle or quadrangle. We will come back to this point later, which at this stage is more of a dimensional analysis but requires further analysis as we shall see when analyzing the fluxes. The considered flow configuration is one of those previously studied in Sections 4 and 5 such that $\alpha_1 = 2$, $p = 3$, $M = 6$, $m = 2$, $k = 10$ mD, $P_e = 5$ bar, $\phi = 0.25$ and $S_{wi} = S_{orw} = 0$.

Figs 7(a), 8(a), 9(a)-(b) and 10(a)-(b) report the saturation profiles $1 - S(\mathbf{x}, t)$ projected on the domain paths indicated in Fig. 6 while Figs 7(b), 8(b), 9(c)-(d) and 10(c)-(d) give the space dependence of the solution by plotting $[1 - S(\mathbf{x}, t)]\, t^{1/\alpha_1}$. In all cases, an excellent agreement between the numerical and the fixed-point solution is observed for late times, specifically from $t/\tau_0 = 511$ for the disk, $t/\tau_0 = 511$ for the square, $t/\tau_0 = 5$ for the rectangle, and $t/\tau_0 = 838$ for the quadrangle.

Now let us look at the flux time evolution over the entire dynamic range. As already explained in Section 5, flux can be computed in two ways: either by the time derivative of the block average saturation, or by the flux at the boundary. Indeed, integrating Eq. (12) on the considered domain Ω, defining the average saturation as $\langle S\rangle(t) = \frac{1}{|\Omega|}\int_\Omega S(\mathbf{x}, t)\, \mathrm{d}\mathbf{x}$ and using Stokes theorem, one gets a NAPL flux (of opposite sign to the water flux) of dimension $L^d T^{-1}$, where d is the space dimension, that reads

$$\Phi_{\mathrm{mf}}(t) = -|\Omega| \frac{\mathrm{d}\langle S\rangle(t)}{\mathrm{d}t} = -\int_{\partial\Omega} D(S)\, \mathbf{n} \cdot \nabla S \, \mathrm{d}\sigma \quad (55)$$

with $\mathbf{n}$ the $\partial\Omega$ outward normal unitary vector and $|\Omega|$ the measure of Ω. In two (three) space dimensions $|\Omega|$ is Ω area (volume), $\partial\Omega$ is its contour (surface) and $\mathrm{d}\sigma$ is an infinitesimal contour (surface) element of $\partial\Omega$.

Flux time evolution, that is more convenient to compute by the average saturation but which we made sure does not depend on the mode of calculation [using the left or right hand side of (55)], is reported in Fig. 11 for all the tested geometries. Whatever the geometry considered, several points are worth noting:

- We observe once again, as in one dimension, an early-time diffusive regime that is characterized by a flux which varies proportionally to $1/\sqrt{t}$, and an anomalous late-time regime that is driven by a flux proportional to $1/t^{(\alpha_1+1)/\alpha_1}$.
- Flux prefactor A_∞ is no longer known analytically as in one dimension, following Eq. (49), but can be quickly obtained numerically from the fixed-point algorithm subject to having an accurate estimate of a finite value of $(t/\tau_0)_\infty$ for which the numerical solution has almost converged to the asymptotic solution for $t \to \infty$.
- The cross-over between the early- and late-time regimes is very narrow. Therefore the early- and late-time asymptotic solutions that dominate completely the fracture-to-matrix dynamic exchange are sufficient to determine the flux over the whole exchange dynamics. In other words, if the asymptotic solutions are determined, then the whole dynamic response of the exchange is also determined to a very good approximation. This remains of course to be demonstrated in practice on more complex geometries than those tested.
- Flux prefactor A_∞ can be computed numerically by a spatial integration of the fixed-point solution. This being said, Fig. 11 clearly shows that fluxes are all translated in time with respect to each other depending on the geometry considered. Only the square and the disk are very close. This means that the relevant characteristic length L_c involved in the diffusion time $\tau_0 = L_c^2/(4D_0)$ remains to be found, instead of setting as we did $L_c = 2R$, L, L_x or L_y depending on whether the medium is a disk, square, rectangle or quadrangle. Once this one is found, if it exists, whatever the geometry considered, all the corresponding fluxes would be in phase and would superimpose if $\Phi_{\mathrm{mf}}(t)/A_\infty$ is considered for $t \to \infty$, following (47). This will be the subject of another work.

To finish with, the constant flux that can be observed at very short times in Fig. 11 for the square and the quadrangle should be discarded because they are artifacts related to the domain discretization, the exchange affecting the first row of cells near the domain boundary only. This was verified by further refining the mesh (the plateau shifts to even shorter times).

7. Summary and discussion

The long-time relaxation of the NAPL saturation inside a matrix block in contact with water was studied in the case of counter-current imbibition for one- or two-dimensional matrix blocks of arbitrary shape. Gravity effects were neglected, so only the pure capillary regime was investigated. The time variations of the matrix-to-fracture transfer flow rate was also studied. The transition from a Boltzmann square-root regime to an "anomalous" algebraic power-law decay was confirmed qualitatively and quantitatively by numerical simulations. In the short-time regime, the semi-infinite assumption is quite robust, so the results may remain useful

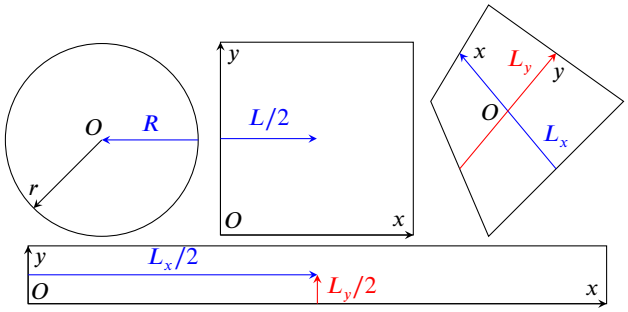

Figure 6: Two-dimensional geometries studied: disk, square, rectangle and quadrangle (all surfaces are to scale except the rectangle, magnified three times). The characteristic lengths as well as the paths on which the saturation field $1 - S(\mathbf{x}, t)$ is projected in Figs 7, 8, 9 and 10 are indicated in blue and red (direction of the path is given by an arrow, coordinate system is shown in black).

even considering general fractured media response in that regime. On the other hand, the long-time decay exponent is directly related to input data combining capillary pressure and relative permeabilities features. As in the long-time regime, the NAPL saturation is uniformly small inside the matrix block, the power-law assumption may be expected to be quite robust, controlled by the low NAPL saturation transport properties. The transition between both regimes is sharp, occurring as soon as the toe of the short-time Boltzmann solution reaches half the block size. The associated matrix-to-fracture flux term $\Phi_{\text{mf}}(t)$ closure may be represented as being proportional to $\langle S \rangle^{\alpha_1+1}$, the exponent α_1 describing the singularity of the diffusion coefficient with NAPL saturation.

For general matrix blocks in 2 dimensions, a similar study was carried out under the same counter-current flow regime. The occurrence of such regime appears to be quite general thanks to a derivation involving the global pressure concept. A similar Ansatz driving the long-time regime was proposed. It predicts a power-law time dependency, and the spatial dependence can be determined numerically using a fast fixed-point algorithm. These findings were confirmed by several comparisons with direct simulations for various typical matrix block shapes. Similar results are obtained for the time evolution of the corresponding matrix-to-fracture flux. A quite sharp transition between a Boltzmann regime involving a $1/\sqrt{t}$ diffusion time-dependence and the anomalous long-time regime driven by the exponent $1/\alpha_1$ can be observed. That transition corresponds to the interplay between the diffusion lengthscale and the characteristic size of the matrix block.

In summary, a promising very fast and accurate computational approach is emerging, which should eventually make it possible, after some additional efforts, to predict counter-current imbibition over a distribution of blocks of various shapes and sizes, which is more representative of naturally fractured porous media. To this end, the following points require further investigation:

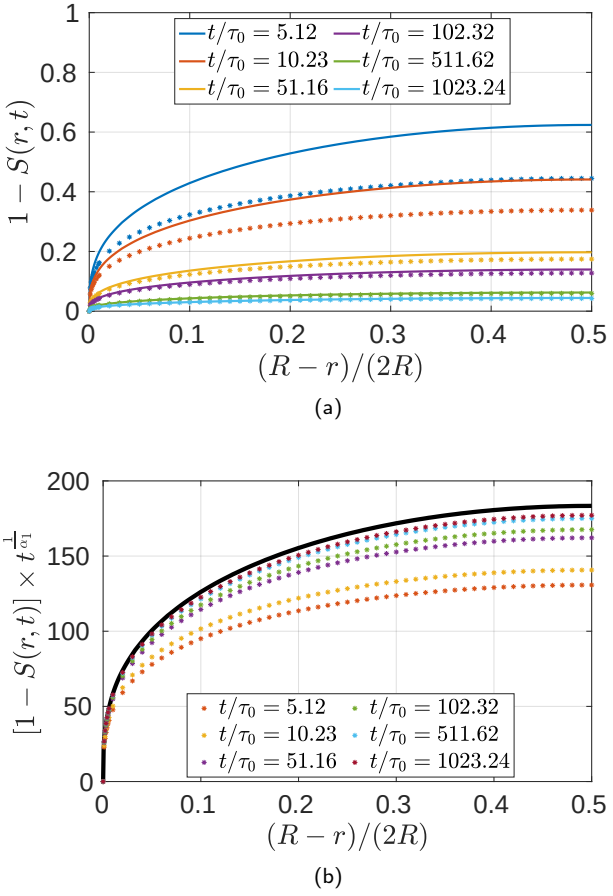

Figure 7: Disk — comparison of the fixed-point solution (solid lines, 1 654 elements) with the numerical solution (symbols, 500 nested rings). Timescale is normalized by the diffusion time $\tau_0 = L_c^2/(4D_0)$ with $L_c = 2R = 1$ m (see Fig. 6).

- A generalization of Parlange's asymptotic early-time solution in any dimension of space might be worth investigating, although nothing simple is apparent at first sight.
- Late-time estimates of $(t/\tau_0)_\infty$, such that the fixed-point asymptotic solution obtained for $t \to \infty$ is valid and the flux prefactor A_∞ is accurately computed, should be consolidated.
- To that end, the relevant characteristic length involved in the diffusion time τ_0 should be determined beforehand as previously discussed, to make $(t/\tau_0)_\infty$ estimates generic (indeed, if the timescale differs from one geometry to another, determining $(t/\tau_0)_\infty$ on a case by case basis may be tedious).

These findings pave the way to research leading to a more faithful description of matrix-to-fracture exchanges when considering a realistic fractured medium composed of a population of matrix block of various size and shapes. In particular, the proportionality constant relating the late-time flux $\Phi_{\text{mf}}(t)$ to $-\langle S \rangle^{\alpha_1+1}$ appears to play a similar role than a shape factor that may be evaluated using single-phase averaging techniques [37, 31, 33]. Looking for simple geometric

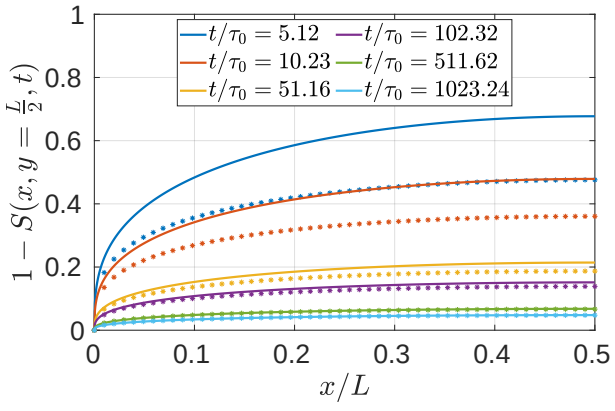

(a)

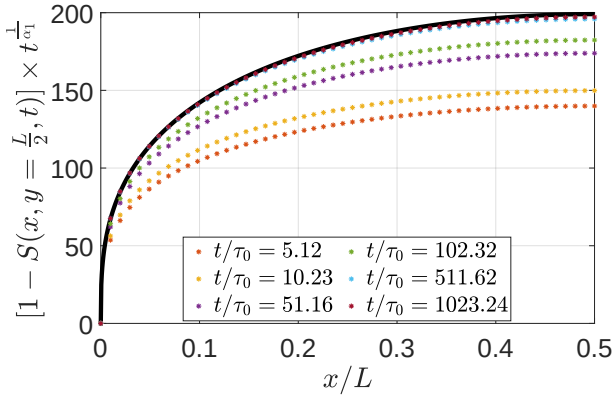

(b)

Figure 8: Square — comparison of the fixed-point solution (solid lines, 4 050 elements) with the numerical solution (symbols, $101 \times 101 = 10\,201$ cells). Timescale is normalized by the diffusion time $\tau_0 = L_c^2/(4D_0)$ with $L_c = L = 1$ m (see Fig. 6).

descriptors quantifying the transition time between diffusion regimes will be of interest for such applications. In parallel, developing averaging methods lumping these various matrix blocks within one macro-scale single exchange flux description will be another research avenue.

A. Appendix: conservative numerical scheme

In this Appendix, we detail the numerical scheme used to solve the singular elliptic partial differential equation (12) in the matrix block domain Ω. We consider neither the Boltzmann variable form (29) for short times, nor the asymptotic form (23) for long times, but the generic PDE (12) that drives the solution $S(\mathbf{x}, t)$ for all $\mathbf{x}$ and t. The singular character of this equation comes from the diffusion coefficient D given by Eq. (13) which vanishes and is not differentiable with respect to S, for $S = \{0, 1\}$, except for particular values of the exponents r, p and q. Because D cancels at the boundary $\partial\Omega$ of the porous medium, one must have $(\nabla S)_{\partial\Omega} = -\infty$ in order to get a non-zero fracture-to-matrix flux $(D(S)\nabla S)_{\partial\Omega}$, as can be seen in Fig. 3. To prevent numerical instabilities or large rounding errors, we set-up a conservative scheme which does not require to compute the product $D(S)\nabla S$, and is based on the following reformulation of Eq. (12) as a conservation law:

$$\frac{\partial S}{\partial t} = \nabla^2 G(S) \quad \text{where} \quad G(S) = \int_0^S D(s)\,\mathrm{d}s, \quad \text{(A1)}$$

with S the normalized mobile aqueous phase saturation (8). The physical domain considered is Ω with boundary conditions $S(\mathbf{x}, t) = 1$ on the boundary $\partial\Omega$ for all $t \geq 0$.

To start with, the function G defined in Eq. (A1) does not admit a simple expression that can be easily handled, except in the limiting cases $M \ll 1$ and $M \gg 1$ (G is then a power-law or an incomplete beta function, respectively) where M is the mobility ratio defined in Eq. (19). To derive a conservative numerical scheme, we resort to a discrete integration of the diffusion function D denoted G^h. To do so, we discretize the normalized saturation interval $[0, 1]$ with the sequence $(\tilde{S}_k)_{k\in\{0,\ldots,N_S\}} = k\Delta\tilde{S}$ composed of $N_S + 1$ points and where $\Delta\tilde{S} = 1/N_S$. For convenience, let us introduce the operator I_G^h which defines the discrete integral of G over two increasing saturation values S_α and S_β. Using the third order Simpson's method, I_G^h writes

$$I_G^h(S_\alpha, S_\beta) = \frac{S_\beta - S_\alpha}{6}\left[D(S_\alpha) + 4D\left(\frac{S_\alpha + S_\beta}{2}\right) + D(S_\beta)\right]. \quad \text{(A2)}$$

For any saturation value S such that $S \in [\tilde{S}_k, \tilde{S}_{k+1}]$, we approximate the function $G(S)$ with $G^h(S) = I_G^h(\tilde{S}_k, S) + \sum_{l=1}^{k} I_G^h(\tilde{S}_{l-1}, \tilde{S}_l)$.

Regarding the domain Ω discretization, let $\mathcal{M}_h$ be an admissible finite volume mesh of the domain Ω given by a family of control volumes or cells noted K: for any K of $\mathcal{M}_h$, $|K|$ is its measure, $KL = \partial K \cap \partial L$ is the common interface between K and a neighbouring cell L. The set of neighbors of cell K is denoted $\mathcal{N}(K)$, that is $\mathcal{N}(K) = \{L \in \mathcal{M}_h; \partial K \cap \partial L \neq \emptyset\}$. Time is discretized with the non-decreasing sequence $\{t^n\}$ such that $t^0 = 0$ and $\Delta t = t^{n+1} - t^n$. Let also S_i^n be the approximation of the saturation on the interval $C_i \times [t^n, t^n + \Delta t)$. Finally, it is useful to introduce the vector $\mathbf{S}^n$ such that $(\mathbf{S}^n)_i = S_i^n$ in order to formulate the scheme vectorially.

Partial differential equation (A1) is recast in a discrete manner with the following finite-volume implicit scheme. Accounting for the boundary condition of an imposed saturation, i.e. $S(x = 0, t) = 1$, $\forall x \in \partial\Omega$, $\forall t \geq 0$, the numerical scheme can be written by introducing the function $\mathbf{Z}^n$ defined for all $K \in \mathcal{M}_h$ as

$$\left[\mathbf{Z}^n(\mathbf{S})\right]_K = S_K - S_K^{n-1} - \sum_{L\in\mathcal{N}(K)} \lambda_{KL}(G_K - G_L) - \lambda_{K,\partial\Omega}(G_K - G(1)), \quad \text{(A3)}$$

with $G_K = G(S_K)$, $\lambda_{KL} = \Delta t|KL|/(|K|d_{KL})$ where $|KL|$ is the face measure and d_{KL} the distance between the center of cells K and L. The term $\lambda_{K,\partial\Omega}(G_K - G(1))$ stands for the boundary condition contributions, non null when the cell K

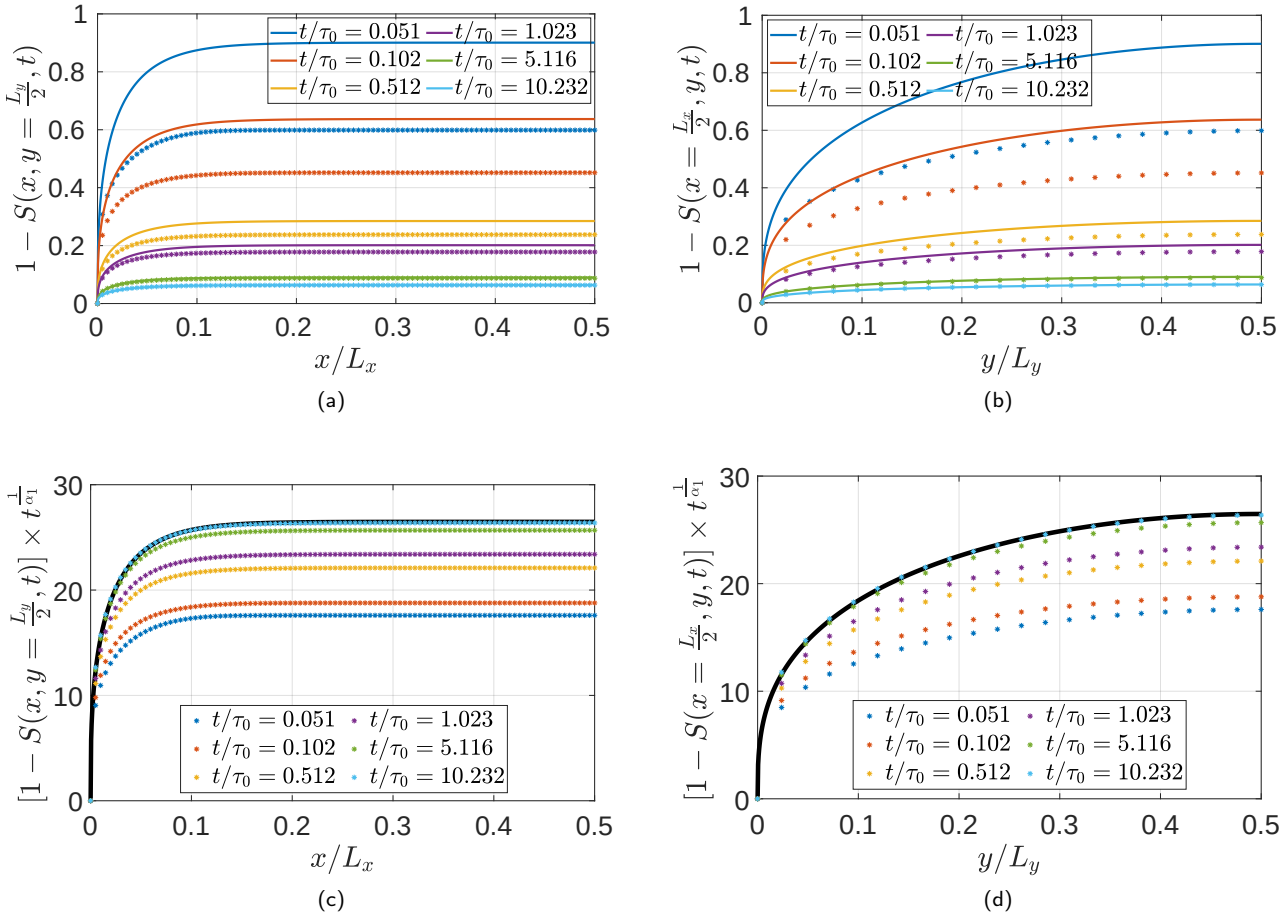

Figure 9: Rectangle — comparison of the fixed-point solution (solid lines, 2 222 elements) with the numerical solution (symbols, $201 \times 41 = 8\,241$ cells). Timescale is normalized by the diffusion time $\tau_0 = L_c^2/(4D_0)$ with $L_c = L_x = 10\,L_y = 1$ m (see Fig. 6).

is a boundary cell. As we use polyhedral mesh cells, it is the sum of several contributions if cell K has several boundary faces. For each boundary face $(\partial K)_j$, that contribution is $\Delta t|(\partial K)_j|/[|K|d_{K,(\partial K)_j}]$ where $|(\partial K)_j|$ is the measure of the face and $d_{K,(\partial K)_j}$ the distance between the cell center and the face.

The updated numerical solution $\mathbf{S}^n$ of this numerical scheme is the zero of the function $\mathbf{Z}^n$. As this function is non-linear because $G(S)$ non-linearly depends on saturation, a Newton-Raphson algorithm is required. Specifically, for each time step we construct a sequence $\mathbf{S}^{n,k}$ such that $\mathbf{Z}^{n,k} = \mathbf{Z}^n(\mathbf{S}^{n,k}) \xrightarrow{k\to\infty} 0$ and recursively defined by $\mathbf{S}^{n,k+1} = \mathbf{S}^{n,k} + \delta\mathbf{S}^{n,k}$ where $\delta\mathbf{S}^{n,k}$ denotes the increment vector given by

$$\delta\mathbf{S}^{n,k} = -\left[\nabla_{\mathbf{S}}\mathbf{Z}^{n,k}\right]^{-1}\mathbf{Z}^{n,k}, \tag{A4}$$

where the matrix $\left[\nabla_{\mathbf{S}}\mathbf{Z}^{n,k}\right]^{-1}$ is the inverse of the Jacobian matrix $\nabla_{\mathbf{S}}\mathbf{Z}^{n,k} = \nabla_{\mathbf{S}}\mathbf{Z}^n(\mathbf{S}^{n,k})$. The increment vector $\delta\mathbf{S}^{n,k}$ is thus determined by solving a linear system. The Jacobian matrix is sparse and its non-null terms are given by, for all $K \in \mathcal{M}_h$:

$$\begin{aligned}\left(\nabla_{\mathbf{S}}\mathbf{Z}^{n,k}\right)_{K,K} &= 1 - \Big(\lambda_{K,\partial\Omega} + \sum_{L\in\mathcal{N}(K)}\lambda_{KL}\Big)D_K^{n,k},\\ \left(\nabla_{\mathbf{S}}\mathbf{Z}^{n,k}\right)_{K,L} &= \lambda_{KL}D_L^{n,k}.\end{aligned} \tag{A5}$$

In addition, as the function G is approximated numerically, we used the function G^h instead of G in relation (A3) to compute the Newton residue $\mathbf{Z}^{n,k}$. To end with, the Newton algorithm is performed until the L^2 norms of the residue $||\mathbf{Z}^{n,k}||_2$ and of the increment $||\delta\mathbf{S}^{n,k}||_2$ are sufficiently small.

A.1. Cylindrical geometry

For a cylindrical domain $\Omega = [0, R] \times [0, 2\pi] \times [0, H]$ invariant by rotation and translation along the z-axis, the solution depends only on the radius $r \in [0, R]$. We therefore consider a uniform mesh composed of $N + 1$ embedded cylinder of first cell $K_0 = [0, \Delta r/2] \times [0, 2\pi] \times [0, H]$ and the following embedded $K_i = [(i - 1/2)\Delta r, (i + 1/2)\Delta r] \times [0, 2\pi] \times [0, H]$ for $1 \le i \le N_K$, where $\Delta r = R/(N_K + 1/2)$. After some straightforward calculations, the scheme writes

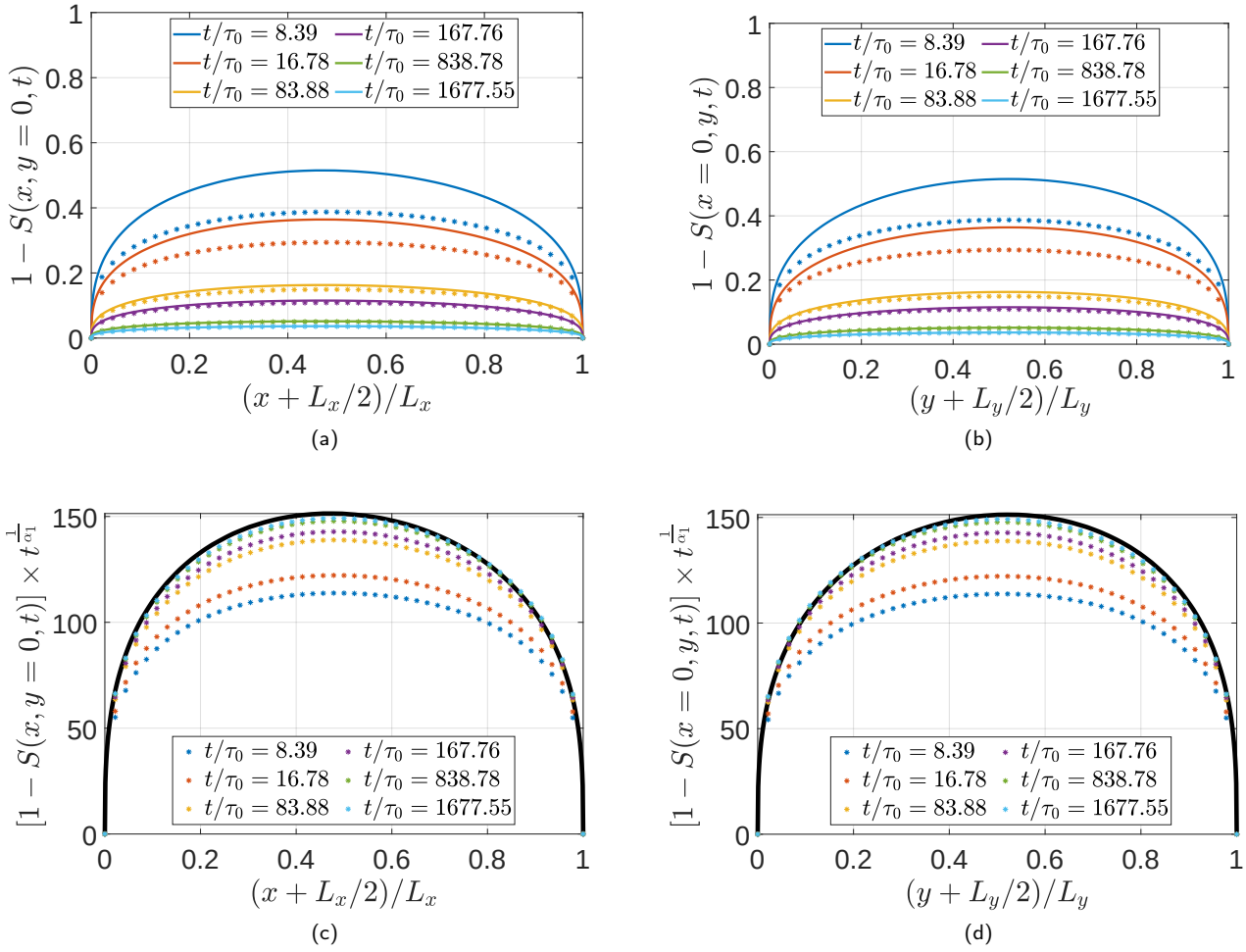

Figure 10: Quadrangle — comparison of the fixed-point solution (solid lines, 4 272 elements) with the numerical solution (symbols, $101 \times 101 = 10\,201$ cells). Timescale is normalized by the diffusion time $\tau_0 = L_c^2/(4D_0)$ with $L_c = L_x = L_y = 0.781$ m (see Fig. 6).

in the form (A3) with

$$\begin{aligned} \lambda_{K_0K_1} &= \tfrac{4\Delta t}{(\Delta r)^2}, \\ \lambda_{K_iK_{i+1}} &= \left(1 + \tfrac{1}{2i}\right)\tfrac{\Delta t}{(\Delta r)^2} \quad \text{for} \quad 1 \le i \le N_K, \\ \lambda_{K_N,\partial\Omega} &= \frac{\Delta t}{\left[1-\left(1-\frac{\Delta r}{R}\right)^2\right]R\Delta r}. \end{aligned} \tag{A6}$$

A.2. Spherical geometry

For a spherical domain $\Omega = [0, R]^3$ invariant by rotation, we consider a uniform mesh composed of $N + 1$ embedded sphere of first cell $K_0 = [0, \Delta r/2]^3$ and the following embedded $K_i = [(i-1/2)\Delta r, (i+1/2)\Delta r]^3$ for $1 \le i \le N_K$, with $\Delta r = R/(N_K + 1/2)$. In this case, the coefficients of the numerical scheme (A3) are

$$\begin{aligned} \lambda_{K_0K_1} &= \tfrac{6\Delta t}{(\Delta r)^2}, \\ \lambda_{K_iK_{i+1}} &= \frac{\left(i+\frac{1}{2}\right)^2}{\left(i+\frac{1}{2}\right)^3-\left(i-\frac{1}{2}\right)^3}\tfrac{3\Delta t}{(\Delta r)^2} \quad \text{for} \quad 1 \le i \le N_K, \\ \lambda_{K_N,\partial\Omega} &= \frac{3\Delta t}{\left[1-\left(1-\frac{\Delta r}{R}\right)^3\right]R\Delta r}. \end{aligned} \tag{A7}$$

References

[1] Abramowitz, M., Stegun, I.A., 1964. Handbook of mathematical functions with formulas, graphs, and mathematical tables. Applied Mathematics Series, National Bureau of Standards. Applied Mathematics Series Vol. 55.

[2] Babu, D.K., van Genuchten, M.T., 1979. A similarity solution to a nonlinear diffusion equation of the singular type: a uniformly valid solution by perturbations. Quaterly of Applied Mathematics , 11–21.

[3] Barenblatt, G.I., Zheltov, I.P., Kochina, I., 1960. Basic concepts in the theory of seepage of homogeneous liquids in fissured rocks [strata]. Journal of applied mathematics and mechanics 24, 1286–1303.

[4] Barenblatt, G.L., Entov, V.M., Ryzhik, V.M., 1990. Theory of fluid flows through natural rocks. Kluwer Academic Publisher.

[5] Barry, D., Parlange, J.Y., Prevedello, C., Loyola, J., Reichardt, K., Nielsen, D., 2010. Extension of a recent method for obtaining exact solutions of the Bruce and K lute equation. Vadose Zone Journal 9, 496–498.

[6] Bouquet, S., Douarche, F., Roggero, F., Leray, S., 2020. Characterization of viscous fingering and channeling for the assessment of polymer-based heavy oil displacements. Transport in Porous Media , 873–906.

[7] Brooks, R.H., Corey, A.T., 1966. Properties of porous media affecting fluid flow. Journal of the Irrigation and Drainage Division 92, 61–90.

[8] Bruce, R., Klute, A., 1956. The measurement of soil moisture diffusivity. Soil Science Society of America Journal 20, 458–462.

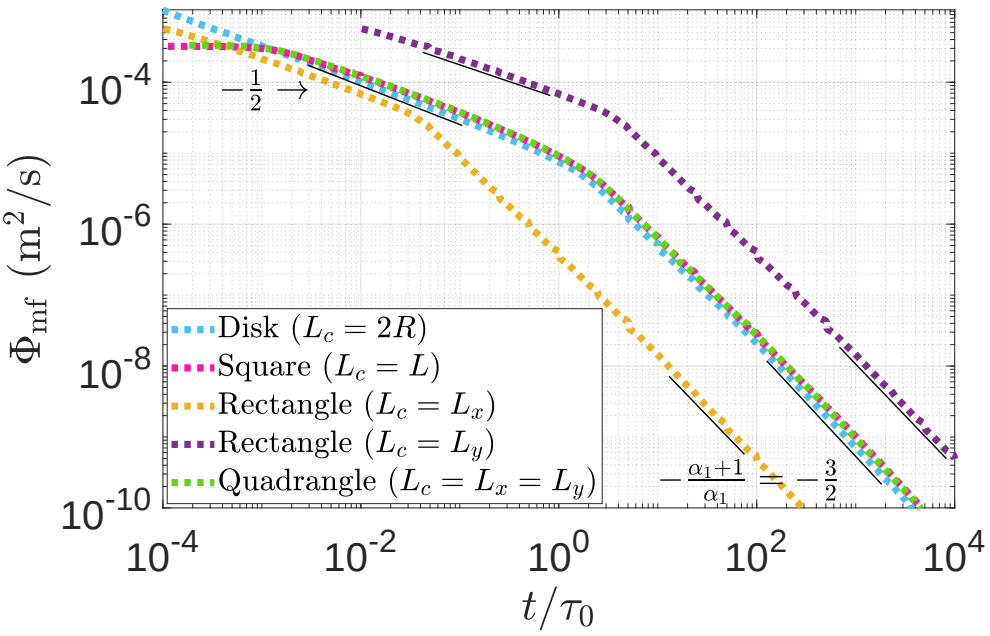

Figure 11: Time evolution of the simulated matrix-to-fracture flux for the considered two-dimensional geometries: disk, square, rectangle and quadrangle (see the text and Figs 7, 8, 9 and 10). Simulated early- and late-time slopes are in excellent agreement with the early- and late-time predictions (thin solid lines) $-\frac{1}{2}$ and $-\frac{\alpha_1+1}{\alpha_1} = -\frac{3}{2}$ for $\alpha_1 = 2$. Timescale is normalized by the diffusion time $\tau_0 = L_c^2/(4D_0)$ where the characteristic length L_c is set to $2R$, L or L_x or L_y depending on whether the medium is a disk (of radius R), square (of side L), rectangle (of sides L_x and L_y) or quadrangle (of medians L_x and L_y). The tested flow configuration is such that $\alpha_1 = 2$, $p = 3$, $M = 10$, $m = 2$, $k = 10$ mD, $P_e = 5$ bar, $\phi = 0.25$ and $S_{wi} = S_{orw} = 0$.

[9] Brutsaert, W., 1968. The adaptability of an exact solution to horizontal infiltration. Water Resources Research 4, 785–789.

[10] Burdine, N.T., 1953. Relative permeability calculations from pore size distribution data. Petroleum Transactions AIME 198, 71–78.

[11] Chavent, G., 1975. Applications of methods of functional analysis to problems in mechanics. Springer. volume 503 of *Lecture notes in mathematics*. chapter A new formulation of diphasic incompressible flows in porous media. pp. 258–270. A new formulation of diphasic incompressible flows in porous media.

[12] Chavent, G., Cohen, G., Jaffre, J., Dupuy, M., Ribeira, I., 1984. Simulation of two-dimensional waterflooding by using mixed finite elements. SPE Journal , 382–390.

[13] Chavent, G., Jaffré, J., 1986. Mathematical models and finite elements for reservoir simulation: single phase, multiphase and multicomponent flows through porous media. Elsevier.

[14] Cherblanc, F., Ahmadi, A., Quintard, M., 2003. Two-medium description of dispersion in heterogeneous porous media: calculation of macroscopic properties. Water Resources Research 39, 1154.

[15] Gennes, P.G.d., Brochard-Wyart, F., Quéré, D., 2004. Capillary and wetting phenomena: Drops, bubbles, perals, waves. Springer-Verlag.

[16] Haggerty, R., Gorelick, S.M., 1995. Multiple-rate mass transfer for modeling diffusion and surface reactions in media with pore-scale heterogeneity. Water Resources Research 31, 2383–2400.

[17] Hansen, A., Flekkøy, E.G., Baldelli, B., 2020. Anomalous diffusion in systems with concentration-dependent diffusivity: exact solutions and particle simulations. Frontiers in Physics 8.

[18] Heaslet, M.A., Alksne, A., 1961. Diffusion from a fixed surface with a concentration-dependent coefficient. J. Soc. Indust. Appl. Math. 9, 584–596.

[19] Hecht, F., 2012. New development in FreeFem++. J. Numer. Math. 20, 251–265. URL: https://freefem.org/.

[20] Jeannin, L., Faille, I., Gallouët, T., 2000. Comment modéliser les écoulements diphasiques compressibles sur des grilles hybrides? Oil & Gas Science and Technology 55, 269–279.

[21] Jerbi, C., Fourno, A., Nœtinger, B., Delay, F., 2017. A new estimation of equivalent matrix block sizes in fractured media with two-phase flow applications in dual porosity models. Journal of Hydrology 548, 508–523.

[22] Kashchiev, D., Firoozabadi, A., 2003. Analytical solutions for 1D countercurrent imbibition in water-wet media. SPE Journal , 401–408.

[23] Lamb, H., 1932. Hydrodynamics. Sixth ed., Cambridge University Press.

[24] Landau, L.D., Lifshitz, E.M., 1987. Fluid mechanics. Second ed., Pergamon Press.

[25] Landereau, P., Nœtinger, B., Quintard, M., 2001. Quasi-steady two-equation models for diffusive transport in fractured porous media: large-scale properties for densely fractured systems. Advances in Water Resources 24, 863–876.

[26] Li, L., Wang, M., Shi, A.F., Liu, Z.F., Wang, X.H., 2020. An approximate analytical solution for one-dimensional imbibition problem in low-permeability porous media. Journal of Porous Media 23, 683–694.

[27] Lomeland, F., Ebeltoft, E., 2008. A new versatile capillary pressure correlation, in: International Symposium of the Society of Core Analysts held in Abu Dhabi, UAE, 29 October - 2 November.

[28] Lomeland, F., Ebeltoft, E., Thomas, W., 2005. A new versatile relative permeability correlation, in: International Symposium of the Society of Core Analysts held in Toronto, Canada, 21-25 August.

[29] McWhorter, D.B., Sunada, D.K., 2011. Exact integral solutions for two-phase flow. Water Resources Research 26, 399–413.

[30] Nœtinger, B., 2015. A quasi steady state method for solving transient darcy flow in complex 3d fractured networks accounting for matrix to fracture flow. Journal of Computational Physics 283, 205–223.

[31] Nœtinger, B., Estebenet, T., Landereau, P., 2001. A direct determination of the transient exchange term of fractured media using a

continuous time random walk method. Transport in porous media 44, 539–557.

[32] Nœtinger, B., Jarrige, N., 2012. A quasi steady state method for solving transient darcy flow in complex 3d fractured networks. Journal of Computational Physics 231, 23–38.

[33] Nœtinger, B., Roubinet, D., Russian, A., Le Borgne, T., Delay, F., Dentz, M., De Dreuzy, J.R., Gouze, P., 2016. Random walk methods for modeling hydrodynamic transport in porous and fractured media from pore to reservoir scale. Transport in Porous Media 115, 345–385.

[34] Parlange, J.Y., Lisle, I.G., Prasad, S.N., Römkens, M.J.M., 1984. Wetting front analysis of the nonlinear diffusion equation. Water Resources Research 20, 636–638.

[35] Parlange, M.B., Prasad, S.N., Parlange, J.Y., Römkens, M.J.M., 1992. Extension of the Heaslet-Alksne technique to arbitrary soil water diffusivities. Water Resources Research 28, 2793–2797.

[36] Purcell, W.R., 1949. Capillary pressure — their measurement using mercury and the calculation of permeability therefrom. Petroleum Transactions AIME , 39–48.

[37] Quintard, M., Whitaker, S., 1998. Transport in chemically and mechanically heterogeneous porous media III. — Large-scale mechanical equilibrium and the regional form of darcy's law. Advances in Water Resources 21, 617–629.

[38] Rose, W., 1999. Relative permeability ideas — then and now (from Richards to Leverett to Yuster, and beyond, in: paper SPE 57 442, SPE Eastern Regional Meeting held in Charleston, West Virginia, 20-22 October.

[39] Silin, D., Patzek, T., 2004. On Barenblatt's model of spontaneous countercurrent imbibition. Transport in porous media 54, 297–322.

[40] Standing, M.B., 1975. Notes on relative permeability relationships. Trondheim.

[41] Tavassoli, Z., Zimmerman, R.W., Blunt, M.J., 2005. Analytical analysis for oil recovery during counter-current imbibition in strongly water-wet systems. Transport in Porous Media 58, 173–189.

[42] Tritton, D.J., 1988. Physical fluid dynamics. Second ed., Clarendon Press, Oxford.

[43] Wyllie, M.R.J., Gardner, G.H.F., 1958a. The generalized Kozeny-Carman equation: its application to problems of multiphase flow in porous, part 1 — review of existing theories. World Oil, Production Section , 121–126.

[44] Wyllie, M.R.J., Gardner, G.H.F., 1958b. The generalized Kozeny-Carman equation: its application to problems of multiphase flow in porous, part 2 — a novel approach to problems of fluid flow. World Oil, Production Section , 210–228.

[45] Wyllie, M.R.J., Rose, W.D., 1950. Some theoretical considerations related to the quantitative evaluation of the physical characteristics of reservoir rock from electrical log data. Petroleum Transactions AIME 189, 105–118.

[46] Wyllie, M.R.J., Spangler, M.B., 1952. Application of electrical resistivity measurements to problem of fluid flow in porous media. Bulletin of the American Association of Petroleum Geologists 36, 359–403.

Nomenclature

Dimensions of the quantities considered are given in parenthesis with M = [mass], L = [length], T = [time], where [#] stands for dimension(s) of #

Vectors are noted in bold

D, mD Darcy, milli-Darcy (unit of permeability, L^2)

1D, 2D, 3D One-/two-/three-dimensional

NAPL Non-aqueous phase liquid

t	Time (T)
$\tau_{0,\mathrm{m}}$	Characteristic time (T)
$\mathbf{x}$	Position in space (L)
x, y, z	Cartesian space coordinates (L)
r	Radial coordinate (cylindrical/spherical geometries, L)
ξ	Boltzmann variable $x/\sqrt{4D_0 t}$ (dimensionless)
∇	Gradient operator (L^{-1})
∇^2	Laplacian operator (L^{-2})
L_c	Characteristic length (L)
L, $L_{x,y}$	Lengths (L)
R	Radius (L)
l_{cap}	Capillary length (L)
ϕ	Porous medium porosity (dimensionless, fraction)
k	Porous medium permeability (L^2)
φ	Subscript denoting either water ($\varphi = w$) or NAPL ($\varphi = o$) phase
ρ_φ	Density of phase φ (ML^{-3})
$\Delta\rho$	Density difference $\rho_w - \rho_o$ between water and NAPL phases (ML^{-3})
μ_φ	Dynamic viscosity of phase φ ($ML^{-1}T^{-1}$)
γ	Interfacial tension (MT^{-2})
θ	Contact angle between fluid and rock (dimensionless)
S_φ	Saturation of phase φ (dimensionless, fraction)
S_{wi}	Irreducible water saturation (dimensionless, fraction)
S_{orw}	Residual NAPL saturation (dimensionless, fraction)
S	Normalized water saturation $(S_w - S_{wi})/(1 - S_{orw} - S_{wi})$ (dimensionless, fraction)
P_φ	Pressure in phase φ ($ML^{-1}T^{-2}$)
P_c	Capillary pressure $P_o - P_w$ between water and NAPL phases ($ML^{-1}T^{-2}$)
P_t	Global pressure ($ML^{-1}T^{-2}$)
$k_{r\varphi}$	Relative permeability to phase φ (dimensionless)
λ_φ	Mobility $k_{r\varphi}/\mu_\varphi$ of phase φ ($M^{-1}LT$)
λ_t	Total mobility (sum of all considered phases mobilities, $M^{-1}LT$)
$\mathbf{u}_t$	Total Darcy velocity (sum of all considered phases Darcy velocities, LT^{-1})
κ_φ	Maximum relative permeability to phase φ (dimensionless)
P_e	Entry capillary pressure ($ML^{-1}T^{-2}$)
p, q, r, m, $\alpha_{0,1}$, u, v	Exponents (dimensionless)
$D(S)$	Saturation S dependent diffusion function (L^2T^{-1})
$D_{0,1}$	Constants that are homogeneous to a diffusion coefficient (L^2T^{-1})
β, γ	Constants (dimensionless)
M	End-point mobility ratio $(\mu_o\kappa_w)/(\mu_w\kappa_o)$ (dimensionless)
$\langle\cdot\rangle$	Space averaging operator (dimensionless)
Φ_{mf}	Matrix-to-fracture flux (LT^{-1})
$A_{0,\infty}$	Matrix-to-fracture flux prefactors ($LT^{-1/2}$)
$B(x; a, b)$	Euler incomplete beta function
$B(x, y)$	Euler beta function
$\Gamma(z)$	Euler gamma function
σ	Shape factor (dimensionless)
Ω, $\partial\Omega$, $\mathbf{n}$	Domain, domain boundary, domain boundary outward normal unitary vector
$\lvert\Omega\rvert$	Measure of domain Ω (L^3, L^2 or L depending on whether Ω is a volume, a surface or a path)

$\|\cdot\|_{2,\infty}$ $\mathcal{L}^{2,\infty}$ norm